AD-A265 054

WHOI-93-09

Woods Hole Oceanographic Institution
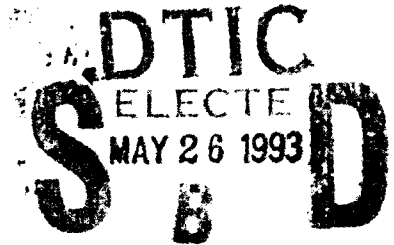
DTIC
ELECTE
MAY 26 1993
S   B   D

Evaluation of Electromagnetic Source for Ocean Climate Acoustic Thermometry at Lake Seneca

by

Mark Slavinsky, Boris Bogolubov, Igor Alelekov, Konstantin Pigalov,
John L. Spiesberger and Paul Boutin

February 1993

Technical Report

93-11845

93 5 25 299

EVALUATION OF ELECTROMAGNETIC SOURCE FOR OCEAN CLIMATE ACOUSTIC THERMOMETRY AT LAKE SENECA

Mark Slavinsky, Boris Bogolubov, Igor Alelekov, Konstantin Pigalov

Institute of Applied Physics of the Russian Academy of Sciences, Nizhny Novgorod, Russia

John L. Spiesberger, Paul Boutin

Woods Hole Oceanographic Institution, Woods Hole, MA. 02543
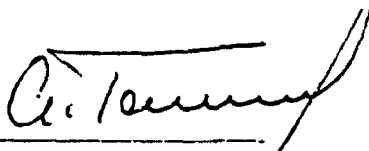
1 February 1993

Technical Report
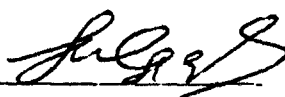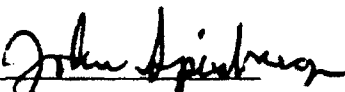
Approved for Distribution:

Prof. Andrey Gaponov-Grekhov
Director, Institute of
Applied Physics
N. Novgorod, November 20 1992

Dr. Craig Dorman
Director, Woods Hole
Oceanographic Institution
Woods Hole, November 20, 1992

Mark Slavinsky
Principal Investigator

John Spiesberger
Principal Investigator

George V. Frisk, Chairman
Department of Applied Ocean
Physics & Engineering

TABLE OF CONTENTS

ABSTRACT

A compact electromagnetic monopole source, requiring pressure equalization, was evaluated at the Naval Underwater Systems Center at Lake Seneca during July 1992 by scientists from the Institute of 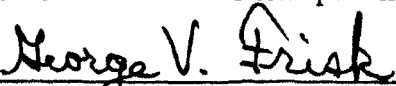Applied Physics of the Russian Academy of Sciences (IAP RAS) and from the Woods Hole Oceanographic Institution and other American organizations. The titanium source was developed at the IAP RAS. The source has a mass of 123 kg and a diameter of 0.54 m. The source cannot be thought of as a single unit; rather the characteristics of the transmitted signal depend on a transmission system consisting of the source, the power amplifier, and a computer. The computer and the amplifier send specially adapted signals to the source to produce the desired acoustic signals. Measurements indicate the acoustic system has a center frequency of 225 Hz, a bandwidth of about 50 Hz, an associated pulse resolution of about 0.02 s, a source level of about 198 dB re 1 μPa @ 1 m, with an efficiency of about 50%. The system has an efficiency of about 67% near 225 Hz, the resonant frequency. The source is suitable for mounting on autonomous ocean moorings for several years as part of a system of monitoring climatic temperature changes over basin scales.

1. INTRODUCTION

It has been suggested that new acoustic technology will make it less expensive to monitor temperatures in the interior of the global oceans than to monitor temperatures in the global atmospheres at scales important for climate change; that is at the largely unexplored scales between the meso and basin scales (Spiesberger, 1992,1993; Spiesberger and Bowlin, 1993; Spiesberger and Metzger, 1992; Spiesberger et al., 1992). The new technology is based on sources attached to autonomous moorings and receivers dangled below freely drifting surface units. An important piece of this new technology is an acoustic source developed in 1991 at the Institute of Applied Physics of the Russian Academy of Sciences (IAP RAS). This report documents the testing of one of these sources at Lake Seneca during July 1992 by IAP RAS and WHOI. Similar sources have been used for more than ten years in scientific work in Russia (Bogolubov et al., 1986; Slavinsky et al., 1992).

We found the sources to be suitable for monitoring climatic temperature changes over basin scales in the ocean. In particular, they had a source level of about 198 dB re 1 μPa @ 1 m, a bandwidth of about 50 Hz, a corresponding temporal resolution of about 1/(50 Hz) = 0.02 s, and efficiencies of about 50%. These sources could be adapted for autonomous operation on moorings for periods of two years with modest sized battery packs.

According to the Agreement on Scientific and Technical Cooperation in the Field of Investigating Global Climate Change using acoustic tomography between the IAP RAS, Nizhny Novgorod, Russia, and WHOI, Woods Hole, MA, USA, joint tests of the low - frequency hydroacoustic sources and driving equipment developed at the IAP RAS were made in July, 1992. During the first stage, from 12 to 24 July, 1992, these groups measured the characteristics of five sources in water of about 16 m depth from the WHOI dock. During the second stage, from 26 to 30 July, 1992, the sources were

evaluated on the barge at Lake Seneca operated by the Naval Underwater System Center (NUSC).

The participants at both stages were

1. From the IAP RAS:

   (a) M. Slavinsky, Deputy Director of the Hydrophysics and Hydroacoustics Department, Head of the Ocean Acoustics Division

   (b) B. Bogolubov, Head of the Applied Hydroacoustics Laboratory of the Ocean Acoustics Division

   (c) I. Alelekov, Research Associate of the Applied Hydroacoustics Laboratory

   (d) K. Γ·galov, Research Associate of the Applied Hydroacoustics Laboratory

   (e) G. Maslakov, Leading production-process engineer of the Design and Technology Section of the Ocean Acoustics Division

2. From WHOI:

   (a) J. Spiesberger, Associate Scientist

   (b) P. Boutin, Research Specialist

3. Other participants during the second stage were:

   (a) K. Metzger, U. of Michigan

   (b) B. McTaggart, Naval Underwater Warfare Center (NUWC)

   (c) J. Lindberg, Naval Underwater System Center (NUSC)

   (d) D. Webb, Webb Research Corporation

   (e) L. Carlton, Director of NUSC Lake Seneca Facility

2. OBJECTIVES AND TASKS OF THE TEST

We refer to the acoustic source, the amplifiers, and the computer controller as the system. Optimum source level, bandwidth, efficiency, and acoustic waveform depends on proper coordination and adaptation of the different system components. The source cannot be evaluated without full consideration of the interactions in the system.

The main objectives of the tests are as follows:

(a) Development of consistent methods that can be used in the future for testing low-frequency hydroacoustic systems by the Russian and American specialists.

(b) Calibration measurements of the characteristics of the system. Measurements include source level, phase and frequency characteristics, efficiency, etc.

(c) Investigation of the characteristics of the system by generation of M-sequence codes that are used for studying global climate changes of temperature using acoustic tomography. Cross-correlation techniques are used to estimate the time resolution and bandwidth characteristics of the system.

(d) Investigation of the influence of the source's hydrostatic pressure compensation system on the source's output characteristics.

(e) Investigation of the effects of pressure imbalances between interior and exterior pressure of the source.

(f) Investigation of starting the system at ambient water temperature; or the so called "cold start" test.

Knowledge of these characteristics is important for evaluating the potential of these systems for use in tomographic monitoring of global ocean temperatures.

3. DESCRIPTION OF THE TRANSMISSION SYSTEM

The transmission system includes:

(a) An electromagnetic hydroacoustic source.

(b) A thyristor power amplifier that produces current in the source electromagnet coil. This amplifier is called an inverter in what follows.

(c) A computer with a input and output modules that provides the acquisition of input signals and the formation of signals that are output to the inverter.

(d) Measuring instruments for electric and acoustic signals.

(e) A hydrostatic pressure compensation system that keeps the gas pressure in the internal source cavity equal to the hydrostatic pressure at the source location depth.

(f) Underwater and surface electric cables.

The transmission system is shown in Figure 1. The subwater part of this system contains the source (1), measuring hydrophone (2) and compensator (3). The field coil of the source is connected to the power output of inverter (4) by a multiple-conductor cable (5) of CWD type with longitudinal hermetization. All conductors in the cable are combined into two ones in order to decrease the ohmic resistance. D.C. voltage is fed to the inverter from the power rectifier (8), which is switched to the three-phase line. The IAP RAS hydrophone is connected through the cable (6) to the input module built into the computer (7), to which a signal proportional to the source coil current (source current) is also supplied. The signal formed by the output module of the computer is fed to the inverter input. All electric signals are measured by the computer and, independently, by the measuring instruments listed below.

3.1 Source

A low-frequency hydroacoustic source of electromagnetic type was tested. A sketch of this source is shown in Figure 2. The source has two round emitting membranes (1) with a special profile to minimize the mechanical loads due to bending, a case which supports the fixed part of the electromagnet core (3); each of the two moving parts of the electromagnet core (4) are rigidly fixed to the

1 - Source

2 - Hydrophone

3 - Compensator

4 - Invertor

5 - Power Cable

6 - Hydrophone Cable

7 - Computer

8 - Power Rectifier

A,V - Measuring Devices
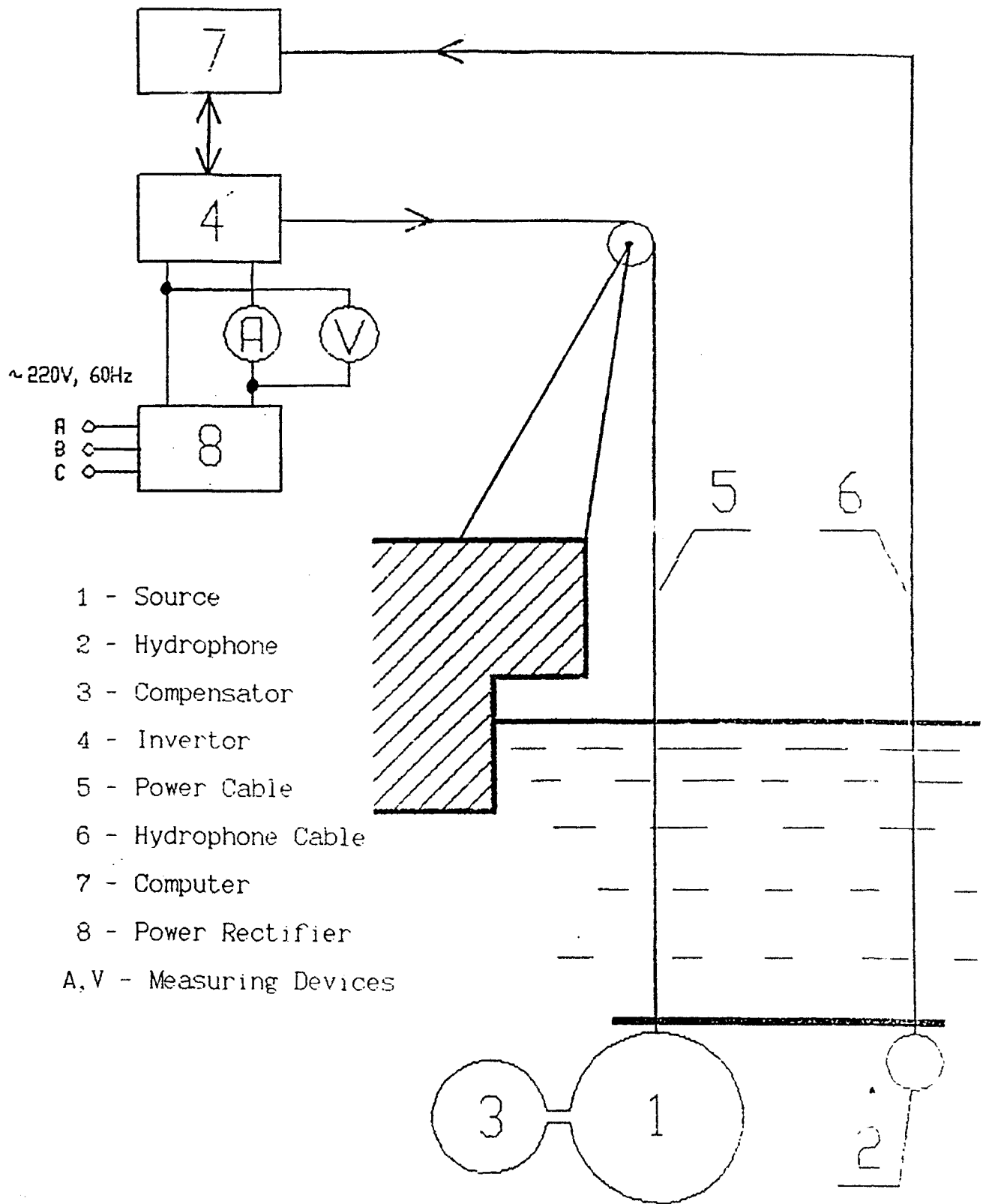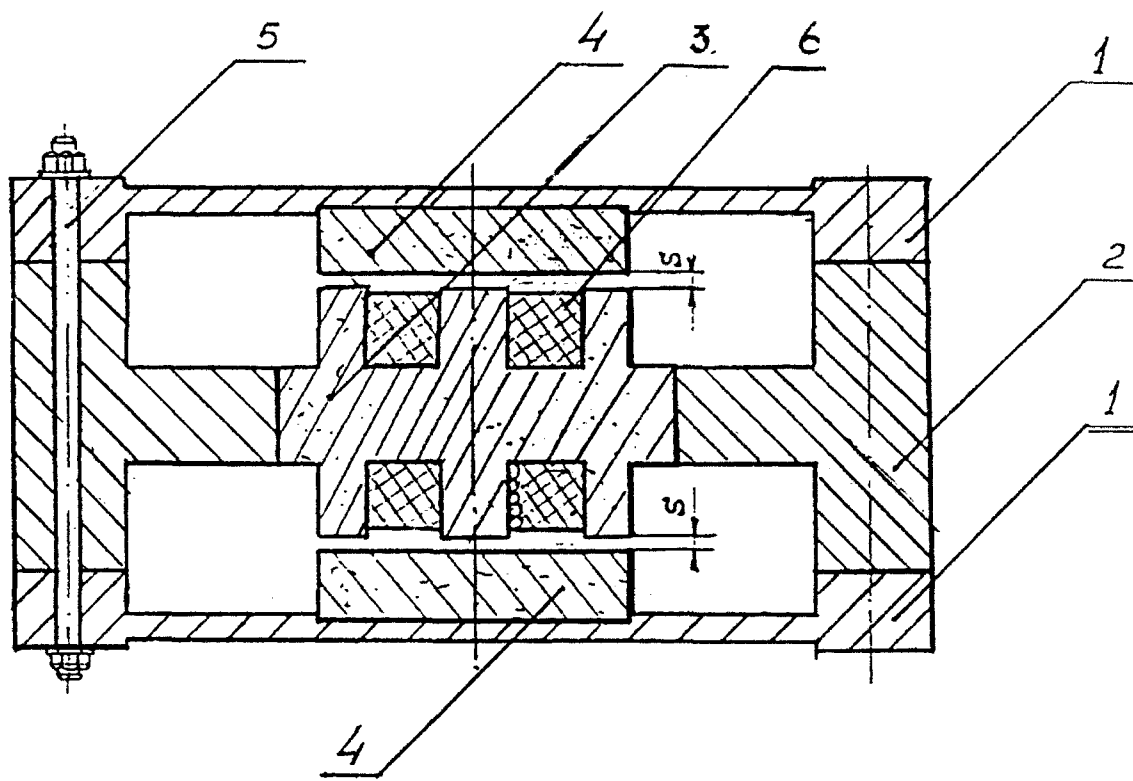
Figure 1: Configuration of the emitting complex.

1 - Membrane

2 - Case

3 - Electromagnet Core (fixed part)

4 - Electromagnet Core (moving part)

5 - Bolts

6 - Field Coil

S - Gap between field poles

Figure 2: Low-frequency hydroacoustic titanium source of electromagnetic type.

center of the corresponding membrane. The membranes and the case are rigidly integrated through the outer flange by bolts (5). The source is made of high - resistant titanium alloys for high reliability and long - term operation in sea water. The membrane oscillations are co - phased so that source behaves like a monopole. The linear dimensions of the source (0.5 m) are much less than the lengths of the acoustic waves it produces (6 - 7 m); therefore the directional pattern of the emitted acoustic field is spherical with high accuracy provided,

$$r >> 2d \ , \tag{1}$$

where d is the maximum geometric dimension of the source, r is the distance from the geometric center of the source to the point at which the field is measured. An interesting feature of the electromagnetic emitters is that the force of attraction between the electromagnet poles is proportional to the square of the current supplied to the coil. Consequently, the frequency of forced vibrations of the source is equal to twice the frequency of the coil current and the emitted power is proportional to the coil current raised to the fourth power. On the other hand, the total power of the Joule heat losses in the electromagnet coil and the losses due to remagnetization of the core is proportional to not more than the coil current squared. The above statements imply that the electromechanical coupling coefficient and efficiency of the electromagnetic sources are not constant and increase with increasing source power. This occurs until the core is saturated. After this the efficiency decreases abruptly.

3.2 Inverter

The input impedance of an electromagnetic source of small wave dimension is mainly inductive. Typically, for matching the impedance of the source and the output resistance of the amplifier, a capacitor is switched, either in parallel or in series, to the electromagnet coil. The capacitance is chosen such that the resonance frequency of the resultant electric circuit is equal to half the resonance frequency of the source. This matching makes the narrow frequency band still narrower. The inverter ensures a better matching to the source. As the source frequency is changed, the inverter is used to keep the radiation level constant by increasing the source current. The stabilization effect is the stronger for high - efficiency emitters. Automatic stabilization of the radiation level makes it possible to generate high-quality signals with frequency and phase modulation in a frequency band much wider than the frequency band of the source. The source power is controlled by commutation of the power supply in a manner similar to pulse duration modulation. Let Ts denote the time duration that the power supply is switched to the inverter. As Ts increases, the power from the source increases. The inverter is fed from a D.C. power supply unit of voltage 250

300V. An electric or storage battery, or a rectifier can be used. In this case we used a three-phase rectifier with V = 220 V and f = 50 - 60Hz.

3.3 Computer

Operation and measurement of the transmitting system is controlled by use of a PC/AT 386 computer (Fig. 3). The output module is used for conversion of the frequency , phase and time Ts codes to an electric pulsed signal which goes to the input of the inverter. The input module amplifies the source coil current signal and enhances and filters the hydrophone signal. From the input module the signals arrive at a standard module PCL 718 of containing 12-bit analog-to-digital converters (ADC). Before measurement, the amplification factors of the programmable amplifiers of the input module are chosen automatically such that the ADC ensure the maximum accuracy during the measurement.

The signal sample frequency is 1 - 2 kHz. During calibration of the source, the sample frequencies are 10 and 40 kHz. The results of the signal measurements are used to calculate various parameters such as the frequency dependence of the radiation level, the effective current of the source field coil, the phase of the emitted signal, the efficiency of the source and of the transmission system as a whole, the average current of the power rectifier, etc. The results of the measurements are shown on the computer display.
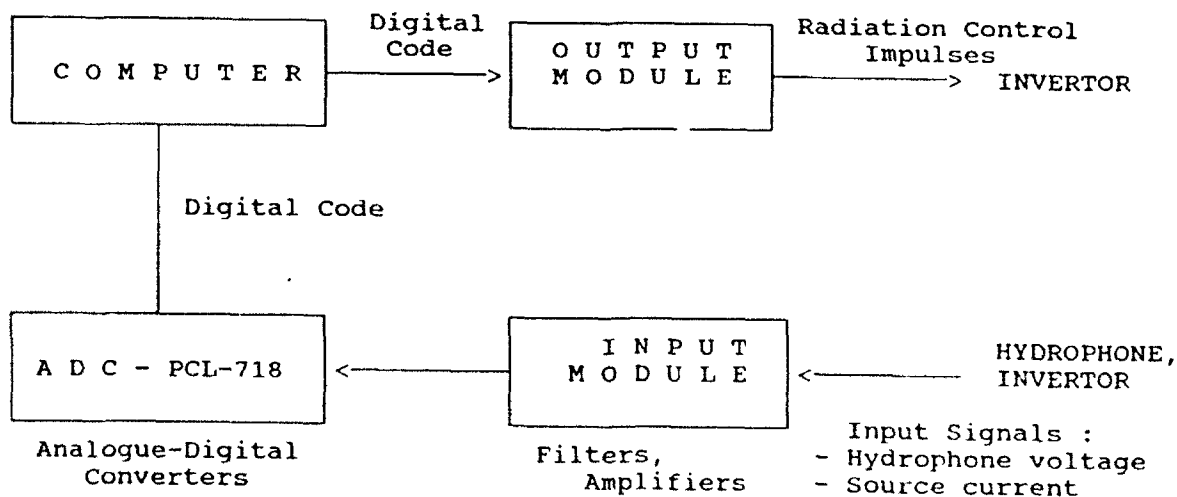

Figure 3:   Structural scheme of the computer complex.

Table 1. Equipment used by the IAP.

Parameters	Measurement Unit	Type of Device	Accuracy of Measurement (%)
Power rectifier voltage	volt	M 42100	1.5
Average consumption current from rectifier	amp	M2027	0.5
Average field coil current of source	amp	M2027	0.5
A.C. voltage on hydrophone	volt	V7 - 27	0.5
Field coil inductance of source	mH	Impedance meter IMF - 600	0.1

3.4 Measuring Equipment

All electric signals are measured by the computer and, independently, by the measuring equipment. The signals being measured and the types of the devices are given in Table 1.

The American colleagues simultaneously measured electric quantities using their own devices listed in Table 2.

The acoustic pressure was measured by three piezoceramic hydrophones, the characteristics of which are given in Table 3.

3.5 Pressure Compensation System

When the source is submerged in water its membranes are bent under the action of hydrostatic pressure, which, at a certain value, can make the source inoperative. The hydrostatic pressure compensation system (PCS) is intended to keep the imbalance between the hydrostatic pressure outside the source and the gas (or air) pressure in the i. 'ernal cavity of the source within admissible limits. IAP used the simplest compensator of the so- called passive type, which is a thick-walled sphere of fiber-glass reinforced plastic divided into two cavities by an elastic diaphragm (Fig. 4). One cavity is connected through holes to the environment and the other cavity is connected to the inner cavity of the source. Since the rigidity of the diaphragm is very small, the pressure in the source is essentially the same as the hydrostatic pressure outside the source

12
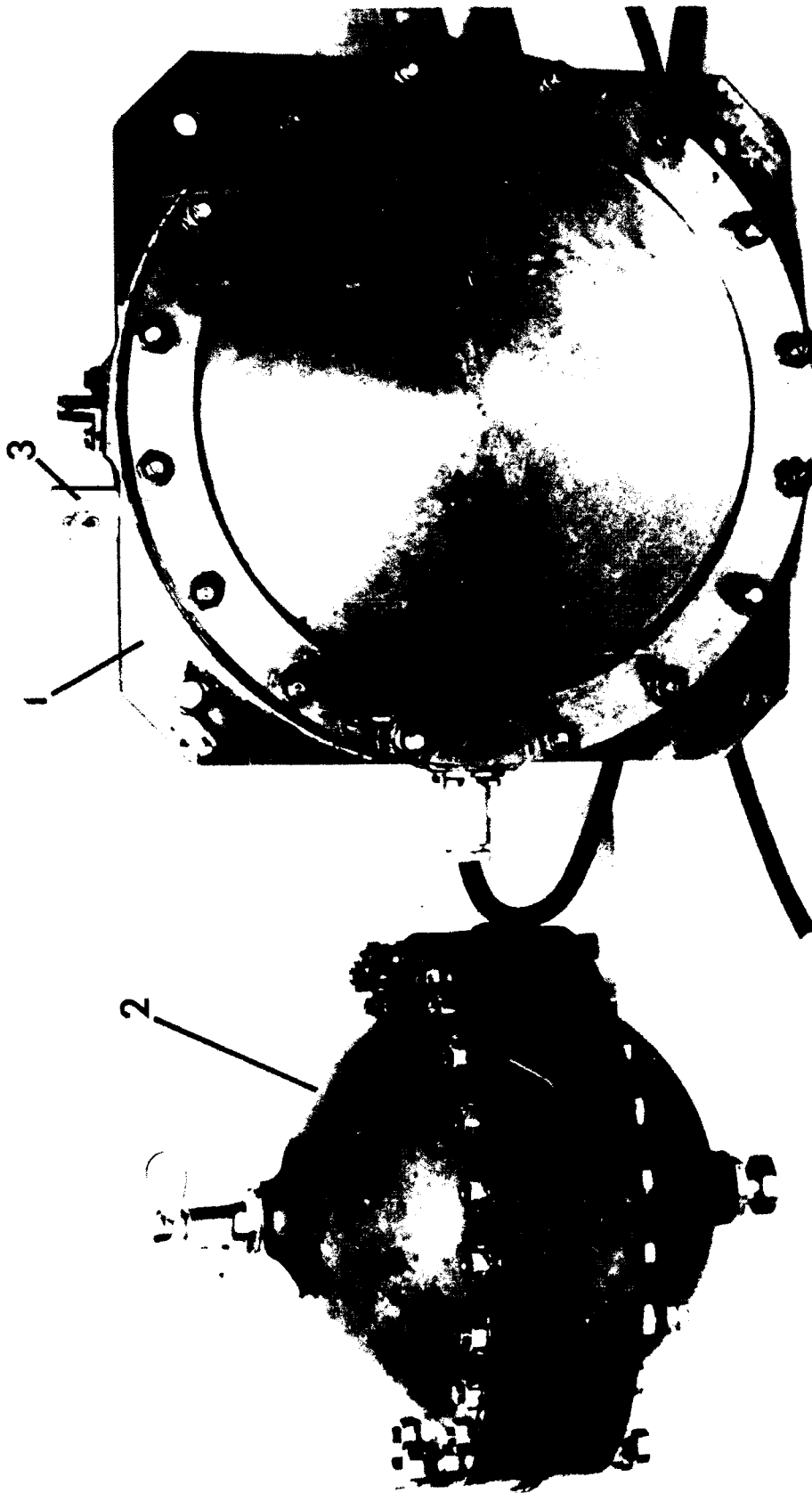
Figure 4: Source with Pressure Compensation System
1 – Source, 2 – Pressure Compensation System,
3 – Match Box

Table 2. Equipment used by the Americans.

Parameters	Measurement Unit	Type of Device	Accuracy of Measurement (%)
Power rectifier voltage	volt	Handheld multimeter Hewlett-Packard E2373	0.7
Average consumption current from rectifier	amp	True rms meter Fluke 87	0.2
A.C. voltage on hydrophone	volt	True rms meter Fluke 8506A	0.1

Table 3. Hydrophone calibrations.

Type of Hydrophone	Serial #	Sensitivity (dB/V re 1 μPa @ 1 m)	Produced by
F37	280	-205.9	Naval Underwater Systems Center Lake Seneca, NY, USA
G3303-M	14	-192.69	Institute of Applied Physics Russian Academy of Sciences Russia
F37	A62	-204.3	Naval Research Lab. Orlando, FL, USA

until water forces the entire gas out of the compensator into the source. In order to increase the depth of submergence, the source and the compensator can preliminarily be pumped with gas (dry air can be used) to admissible pressure. Assume that Vs is the volume of the inner cavity of the source, Vc is the volume of the compensator and Po is the initial gas pressure in both volumes. Then the maximum depth of submergence H (in meters) is,

$$H = 10(Po + (Po + 1)Vc/Vs) \ . \tag{1}$$

In our case, Vc= 17 liters, Vs = 6 liters, Po = 15 atm, H = 600 m. An important parameter of the compensator is the time of pressure equalization, which should be less than the characteristic time of variation of the source depth.

The source mass is 123 kg, the source's diameter is 0.54 m, the PCS mass is 10 kg, and the PCS diameter is 0.450 m. A match box is placed on the top of the source for comparison of size.

4. METHOD OF ACOUSTIC MEASUREMENT

The source was placed in the water using cranes on the NUSC barge. The power and control apparatus of the transmission system were placed in the laboratory while the source, the hydrostatic pressure compensation system and the monitoring hydrophones were submerged using a steel rope. The depth of submergence was measured from the water surface by reading the counter mounted on the winch. Signal measurements were made with Russian and American ammeters, voltmeters, calibrated hydrophones, and data processing equipment. The tests were performed with the source at between 23 and 100 m depth.

The source was tested with and without the hydrostatic pressure compensation system. The hydrological conditions in Lake Seneca were essentially unchanged throughout the tests. Figure 5 shows the typical vertical sound speed profile, which was measured by the NUSC facility at different times. These data were used for determining the efficiency of the system.
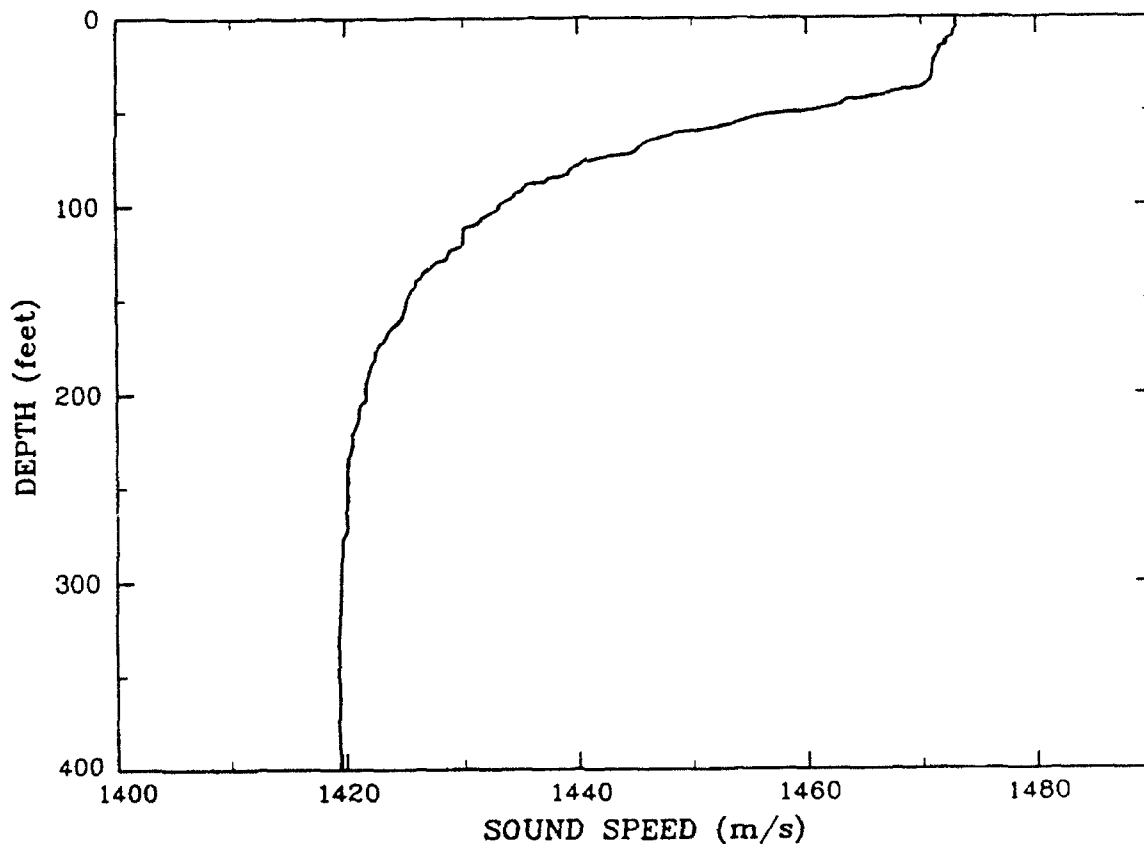

Figure 5: Seneca Lake Sound Speed Profile

Table 4. Check on the consistency of the calibrated hydrophones. Three
hydrophones listed in Table 3 are mounted as shown in Figure 6b, except at
a distance of 1.99 m instead of 2.03 m. The voltages were measured at the
cable terminations provided with each hydrophone. On the 28th of July,
voltages on the F37 hydrophones are measured on the U. of Michigan Fluke
voltmeter using the 2 V scale (model 8050A). On the 29th, voltages on the
F37 hydrophones are measured with the Fluke model 8506A thermal rms
digital multimeter supplied by the facility at Lake Seneca (USN 015185,
serial number 4275008).

Type of Hydrophone	Output (dBV)	28 July Source Level (dB)	Output (dBV)	29 July Source Level (dB)
F37, #280 Seneca	-12.54	199.36	-12.73	199.17
G3303-M #14 Russian	–	198.61	–	198.51
F37, #A62 Orlando	-12.08	198.22	-12.11	198.19

Provisional comparative tests of the hydrophones were performed using acoustic
tones. The results of two typical measurements are given in Table 4.

The largest scatter of values, 1.18 dB, was observed between hydrophones F37 No.
280 and F37 No. A62. Measurements using hydrophone G3303 No. 14 fall about half-
way between the American hydrophones. The general scatter of measured parameters,
about 1 dB, corresponds to the accuracy in calibration. The hydrophones were spaced
$r \geq 2$ m from the geometric center of the source, so that condition (1) was satisfied.

The distance between the source and the hydrophone was fixed by a rigid bar, to
one end of which the hydrophones were fastened and the other end was connected to
the source.

In the first version, the hydrophones were mounted on the end of a pinewood stick
(Fig. 6a). In the second version, a metal rod was used.

The hydrophones and the source were suspended from the ends of the rod (Fig. 6b).
These two versions yielded similar estimates of the transmission system.

Another desirable condition is that emission be made into open water away from
boundaries. This requirement is met if there is a small contribution to the acoustic
field from imaginary sources due to bottom and surface reflections. If the local depth
is H and the depth at which the source is submerged is h, then in the worst case the
influence of these reflections, can approximately be defined from the equation,

$$d = 100(r/2h + r/2(H - h)) \ (\%) \ ,\tag{1}$$

for $r << h$ and $r << H - h$ (Appendix A). In our case, at $r > 2$ m, $H = 130$ m, and $h = 25 - 100$ m, the maximum error in amplitude is $d = 5\%$.

The measurement could be influenced by interactions with the barge and with other transducers in the water during the test. Therefore, the measurement data obtained at the maximum depths of submergence of the source should be considered more reliable than the shallower measurements.
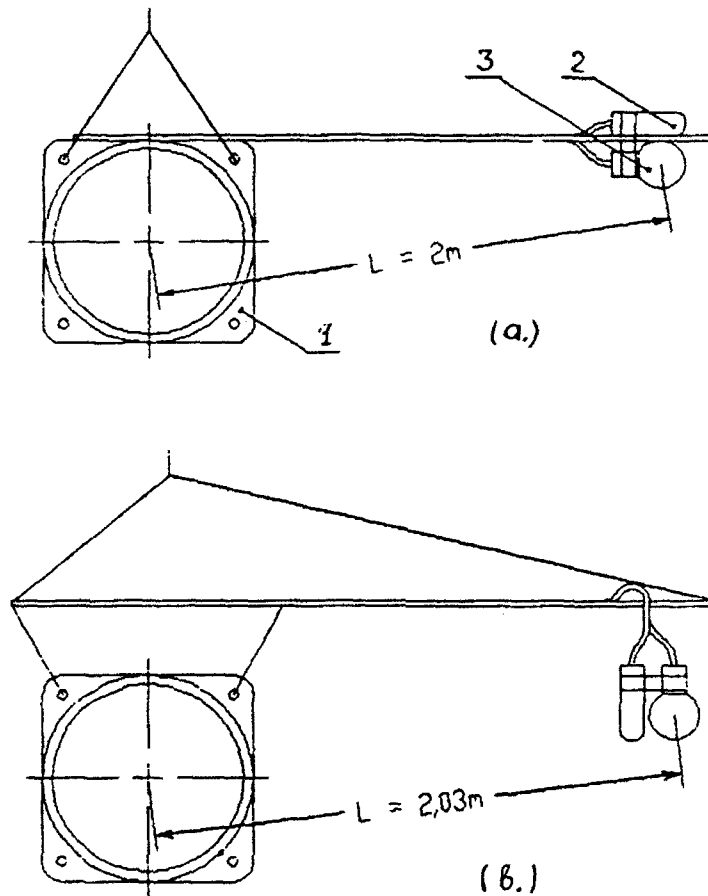
1 - Source.

2 - Hydrophone F37 (USA).

3 - Hydrophone G3302 - M (Russia).

Figure 6: Changes of system configuration
        (a) the first version, (b) the second version

5. CALIBRATION OF THE SOURCE

The objective of source calibration is to define the acoustic parameters of the source and the parameters of the transmission system when different tones are emitted. The calibration is controlled automatically with a computer. The calibration matrix is formed from sequential steps in frequency - output level space. The rows of the matrix indicate frequency and the columns of the matrix indicate the source power parameterized by the commutation time, Ts. The following parameters are set in the computer before calibration :

f_0, minimum source frequency

f_1, maximum source frequency

df, the step in frequency

Ts_0, minimum value of the parameter Ts

Ts_1, maximum value of the parameter Ts

dTs, the step in parameter Ts.

The following parameters are also assigned: the distance between the source and the hydrophone, the sensitivity of the hydrophone, the power supply voltage fed to the inverter, the ohmic resistance of the power cable between the inverter and the source, the sound speed at the depth of submergence, and the water density. After the parameters of the next step are set automatically and the emission is switched on, with a delay of 0.3 seconds, the time needed for the onset of steady state of the source, the computer selects the gains of the input module amplifiers during 60 - 90μs. Thereafter during 0.2 s, the hydrophone is digitized at 10 kHz and the average amplitude and phase of the acoustic pressure is calculated. In the next 0.1 s, the hydrophone and the coil current signals are digitized at 40 kHz and displayed. Also, they are used for calculation of the effective coil current and the average consumption current. In the last period of time, the source radiation is gradually decreased automatically and switched off.

Ten matrix calibrations were taken using different depths of submergence and using the source with and without the pressure compensation system. The parameters for the calibrations and the main results are given in Table 5.

Calibration was performed between 205-240 Hz at a maximum radiation level about 200 dB. Measurements 1-7 were performed without a pressure compensation system (PCS). Measurements 1-2 were conducted for debugging the transmission system and choosing the optimal range of taking the source characteristics.

19

Table 5. Calibration runs on the acoustic source (matrix tests). Run 1 was done using the geometry given in Figure 6a. Runs 2 through 7 inclusive were done using the geometry given in Figure 6b except with hydrophones at a distance of 1.99 m from the center of the source. Runs 8 through 10 were done using the geometry given in Figure 6b. The source depth is H, the minimum, maximum, and increment frequencies are f_0, f_1, and df respectively. The minimum, maximum, and increment pulse durations transmitted to the source are Ts_0, Ts_1, and dTs respectively. The source level at maximum power is SL_m and occurs at the maximum pulse duration. The calculated efficiencies of the source and of the entire transmission system are E_s and E_c respectively. An asterisks indicates the pressure compensation system was used.

#	H (m)	f_0 (Hz)	f_1 (Hz)	df (Hz)	Ts_0 μs	Ts_1 μs	dTs μs	SL_m (dB)	E_s at SL_m	E_c at SL_m
1	30	205	240	1	500	1300	50	196.5	0.567	0.514
2	23	205	240	1	500	1500	50	200.0	0.681	0.623
3	33	205	239	2	600	1500	100	200.3	0.835	0.765
4	34.8	205	239	2	600	1500	100	199.8	0.810	0.743
5	36.6	205	239	2	600	1500	100	199.7	0.837	0.765
6	31.2	205	239	2	600	1500	100	200.2	0.858	0.784
7	29.4	205	239	2	600	1500	100	200.4	0.797	0.725
8*	45.1	205	239	2	600	1600	100	1~~.9	0.746	0.665
9*	75	205	239	2	600	1600	100	19~.8	0.749	0.667
10*	100	205	239	2	600	1600	100	199.6	0.770	0.688

Measurements 3-7 were made for investigation of the influence of the imbalance between the pressures inside and outside the source on its characteristics. In measurements 8-10, the source with the PCS was used. The influence of the depth of submergence on the system was investigated. Figures 7-16 show the results obtained by processing the calibration matrix data on the computer corresponding to line 5 of Table 5. Figure 7 shows the frequency dependence of the radiation level at a constant Ts. The radiation level is not sensitive to frequency thus the emitted bandwidth is wide. At a level of -3 dB from the peak, the frequency band of the source is greater than the frequency range of the calibration (over 35 Hz). Figure 8 shows the frequency dependence of the radiation level at a constant value of coil current . The radiation band is narrower and is close to 12 Hz.

The conditions for measurement of the amplitude-frequency dependence at a constant value of coil current approximately correspond to excitation of a mechanical oscillation of the source by a constant force. Thus, Figure 8 shows the resonance characteristics of the source. Figures 7 and 8 show the importance of adapting the signal for the source to create a transmission with a wide bandwidth.
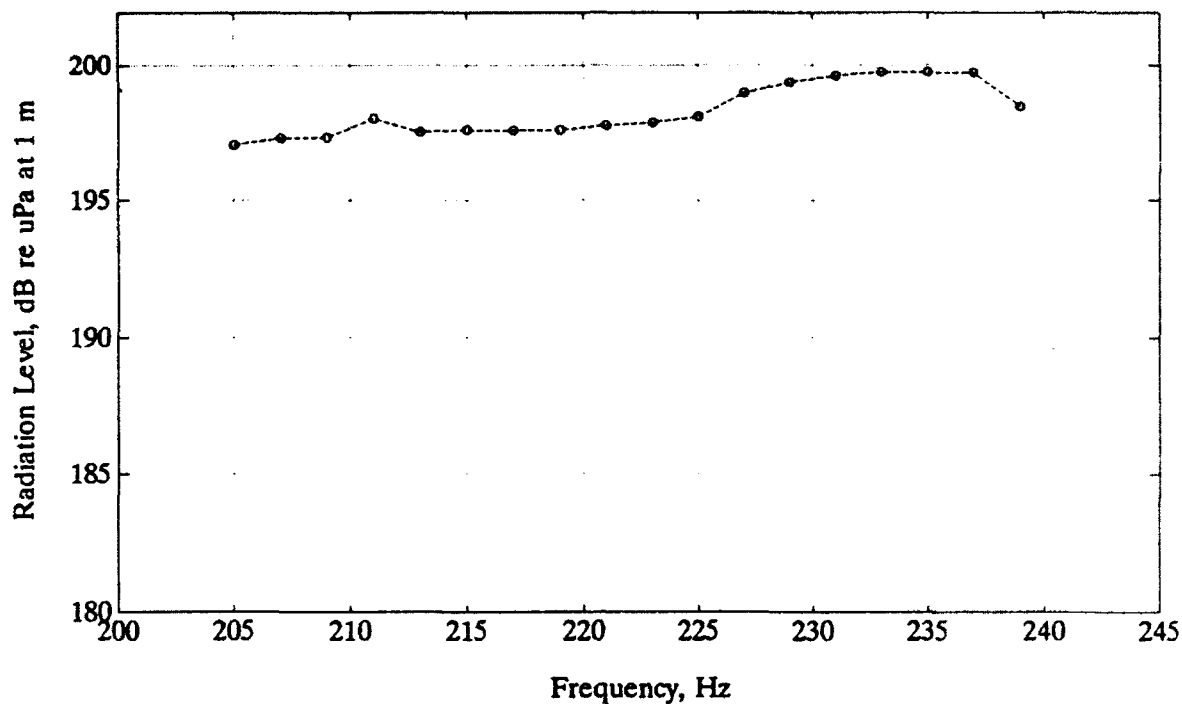
20

Figure 7: Frequency dependence of radiation level at constant Ts = 1500 microsec; Ts is the input pulse duration
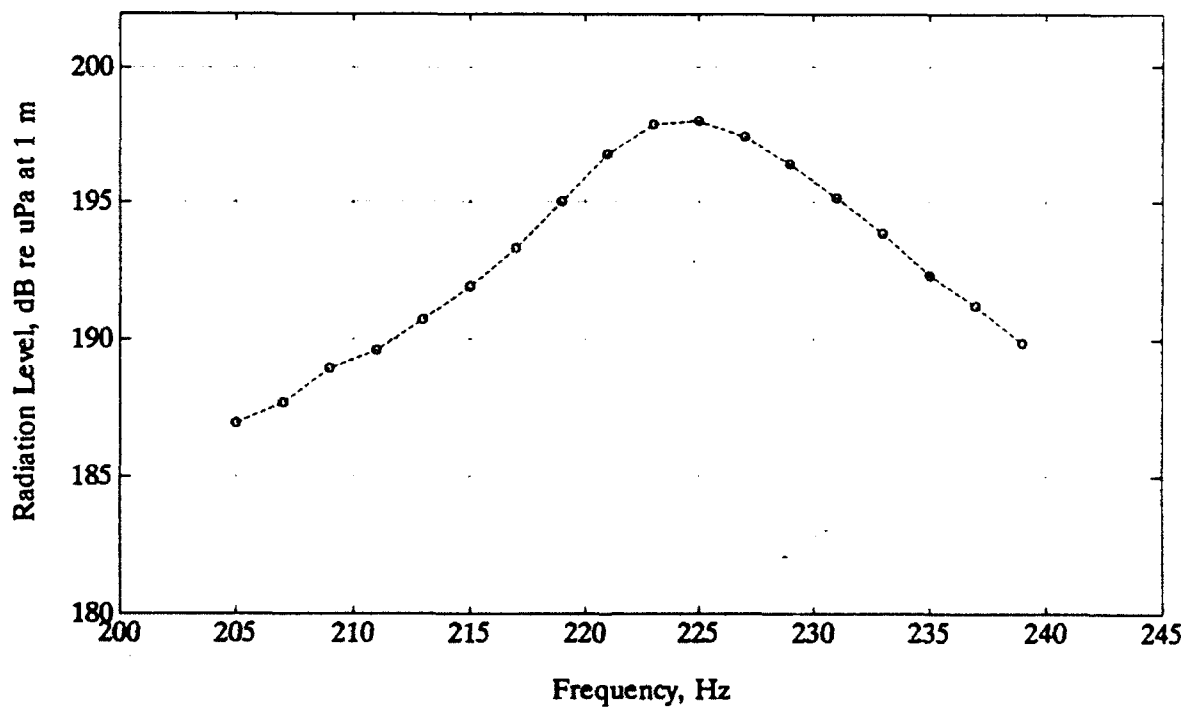

Figure 8: Frequency dependence of radiation level at constant source current Ir = 5.3 A.

21

Figure 9 displays the frequency dependence of the coil current at Ts = constant using the same conditions shown in Figure 7. The coil current increases when the source is detuned from resonance while the radiation level changes little. Figures 10 and 11 exhibit the dependencies of the source radiation phase on frequency and on Ts, respectively. The curve in Figure 10 corresponds to the classical dependence of the oscillator phase with frequency. The dependence of the radiation phase on Ts is weak (Fig. 11). Figures 12 and 13 present the dependencies of the radiation level on Ts and on coil current. Figures 14 and 15 show the dependencies of the source efficiency on frequency and on Ts respectively. Frequency dependence of the efficiency of the system as a whole is demonstrated in Figure 16. It is seen from these figures that the source efficiency increases together with the radiation level and decreases with the departure from resonance. The source efficiency is calculated by,

$$Es = Wa/(Wp - Wi - Wc) \;, \tag{4}$$

and the efficiency of the transmission system as a whole is calculated by,

$$Ec = Wa/Wp \;, \tag{5}$$

where Wa is the acoustic power of the source, Wp is the power consumed from the source, Wi is the power dissipated in the inverter, and Wc is the power lost in the power cable.

Using the results of the calibration we can make a few generalizations about the parameters of the transmission system at a radiation level about 200 dB:

Resonance frequency of the source	225 Hz
Acoustic bandwidth of the system	> 35 Hz
Variation in the freq. response of the source in the range 205 - 240 Hz	< ± 1.5 dB
Average efficiency of the source using IAP calibrations at different depths	≅ 75%
Average efficiency of the system using IAP calibrations at different depths	≅ 66%.

The characteristics of the calibration matrices remained almost unchanged when the PCS was attached to the source. For example, the radiation level changes little at resonance when the PCS is attached (Fig. 35).
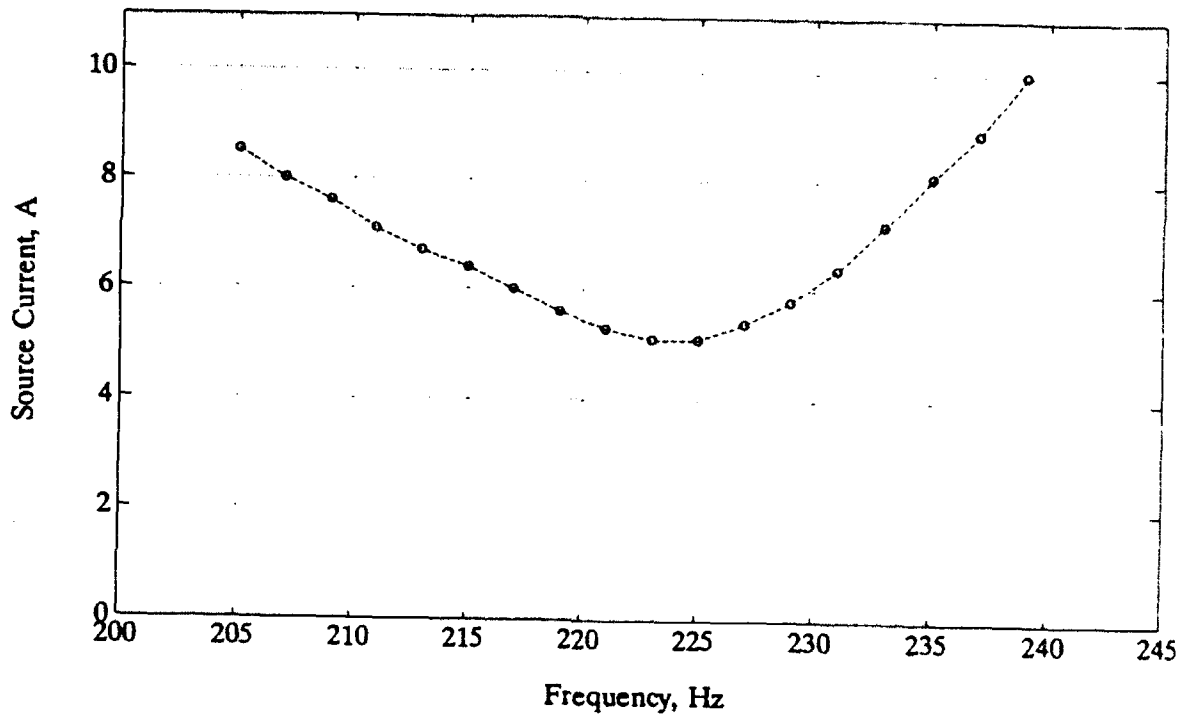
Figure 9:   Frequency dependence at the source current at
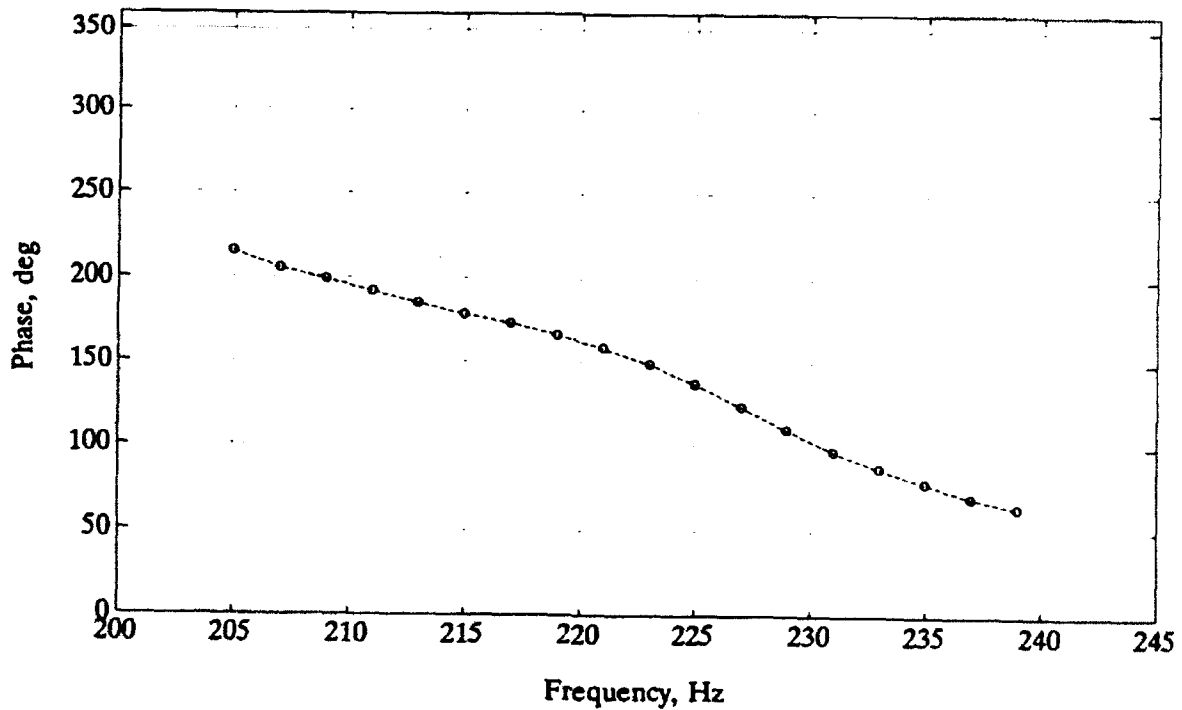   constant Ts = 1500 microsec.

Figure 10: Frequency dependence of emitted signal phase at
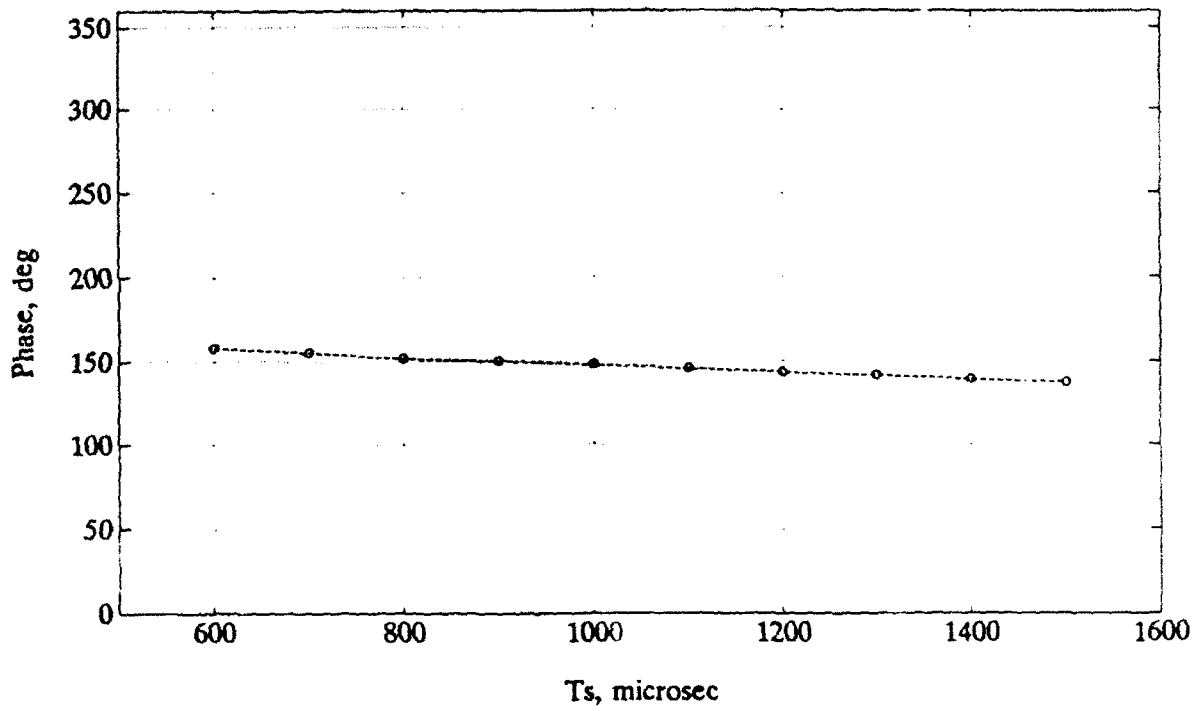   constant Ts = 1500 microsec.

23

Figure 11: Phase of emitted signal as a function of Ts
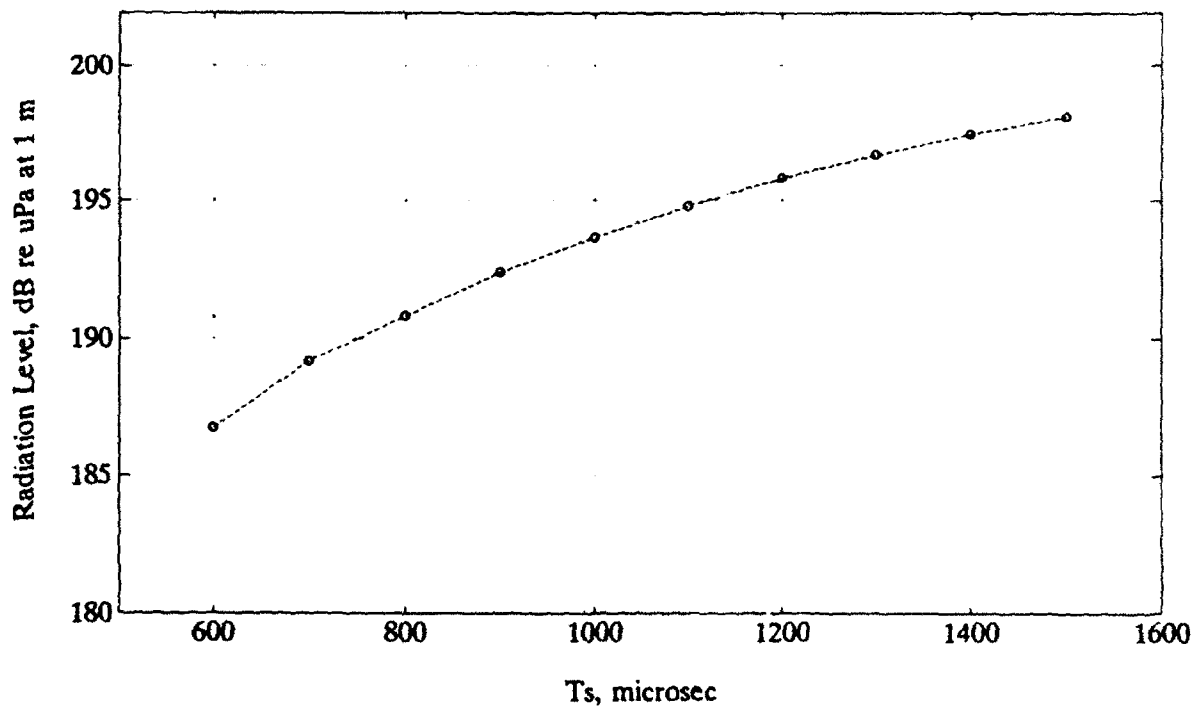at constant frequency 225 Hz.

Figure 12: Radiation level as a function of Ts at constant
frequency 225 Hz.

24

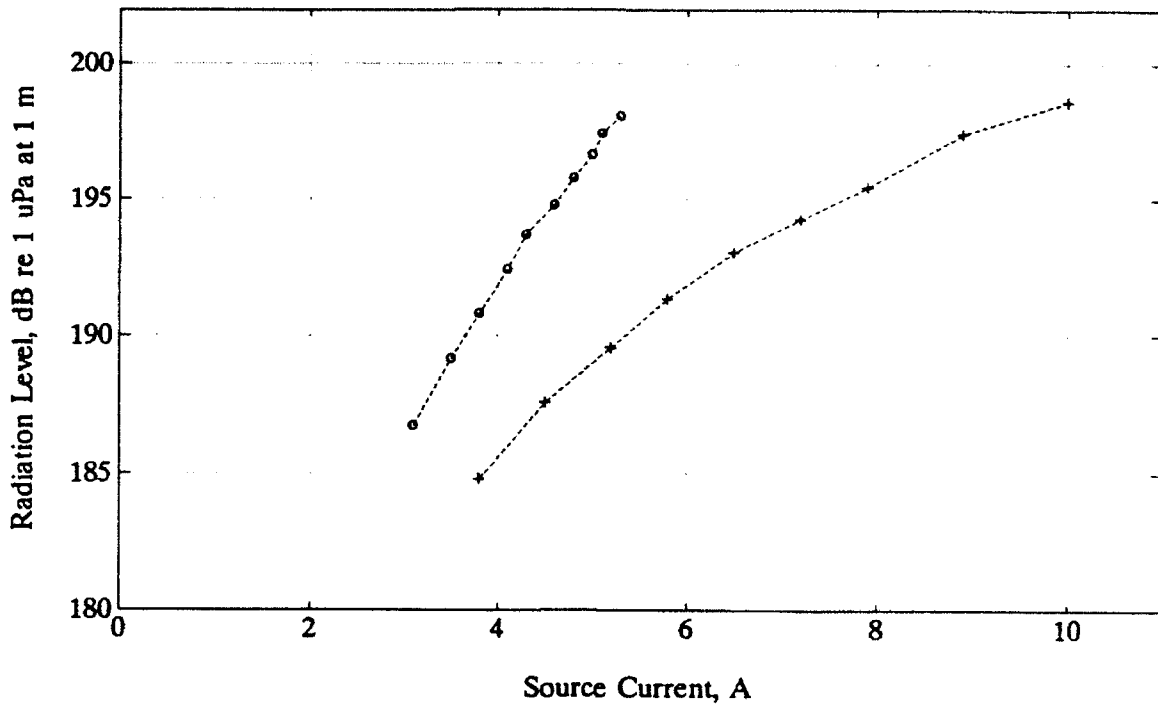Figure 13: Radiation level as a function of coil current at constant frequency: 0-225 Hz (resonance), + - 239 Hz.
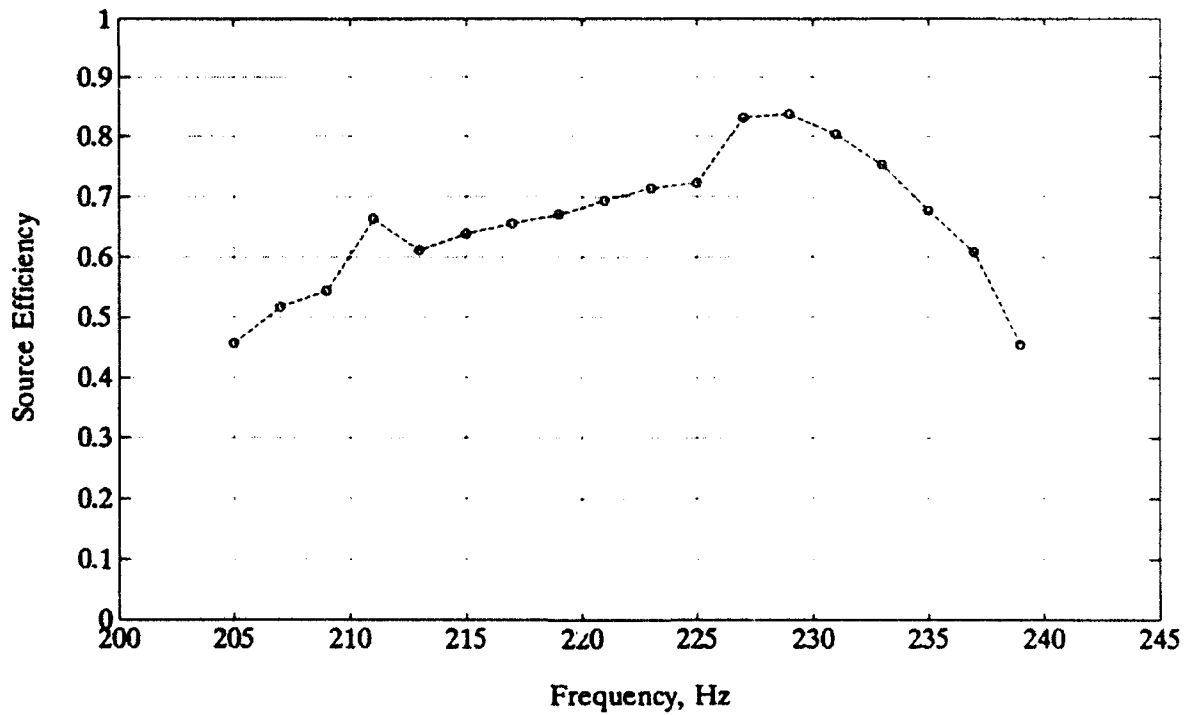

Figure 14: Frequency dependence of source efficiency at constant Ts = 1500 microsec.
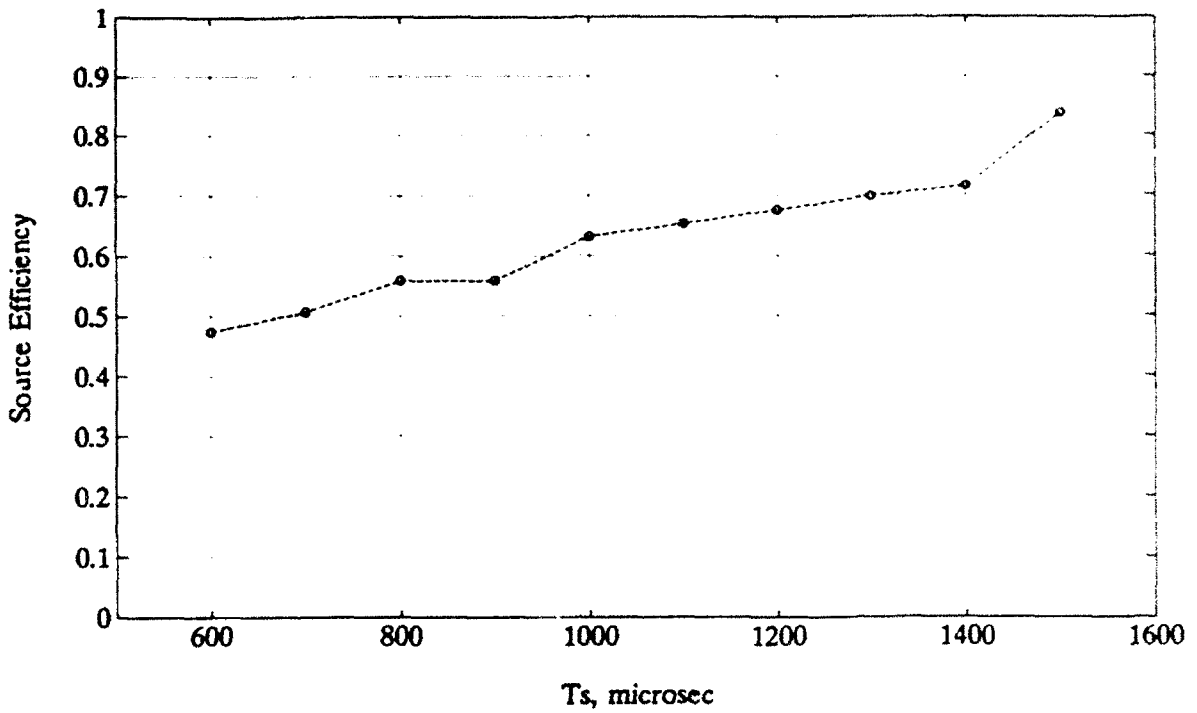
25

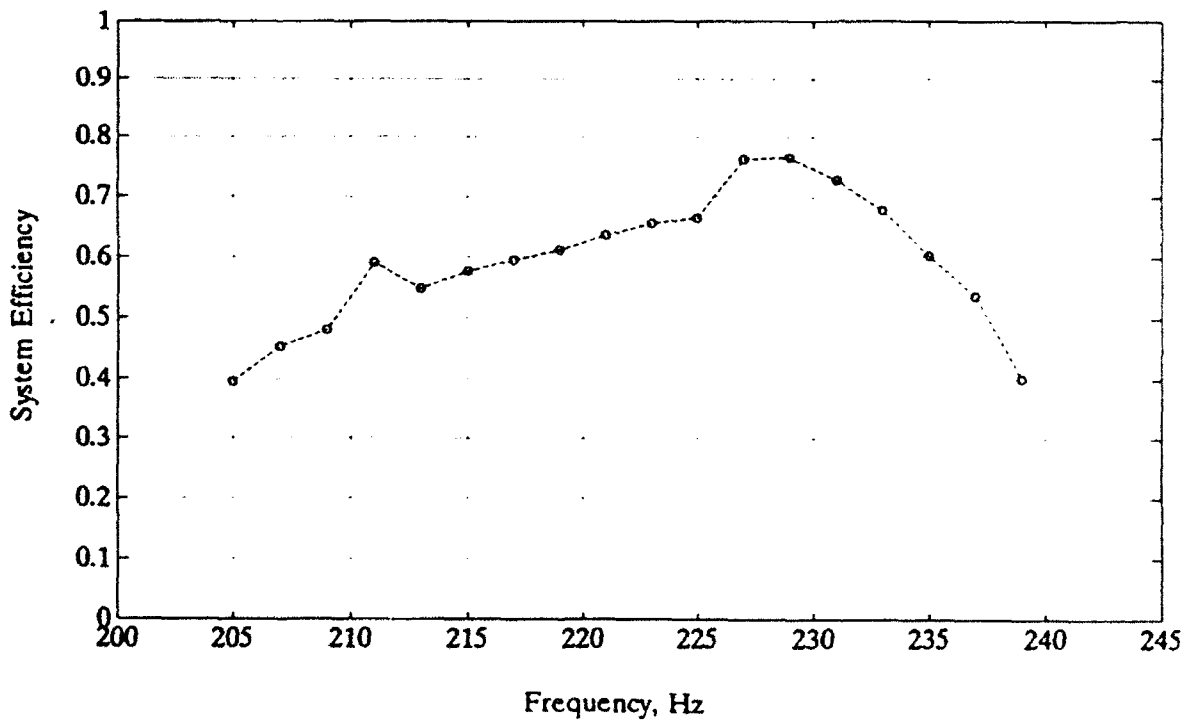Figure 15: Source efficiency as a function of Ts at constant frequency 225 Hz.

Figure 16: Frequency dependence of system efficiency (efficiency of the emitting complex as a whole) at constant Ts = 1500 microsec.

6. TRANSMISSION OF CODED SIGNALS FOR OCEAN ACOUSTIC TOMOGRAPHY

A main feature of the transmission system is the transmission of coded signals. M-sequences and frequency-modulated signals were emitted. With M-sequences, the computer signals were formed by the algorithms developed at the IAP or were formed using K. Metzger's BCSG80 K. Metzger made an electronic unit which converted the output of the BCSG80 to an output suitable for input to the IAP inverter.

During transmissions, the computer was not used to measure the coil current; therefore the currents and power supply voltages were determined by reading the instruments labelled A and V in Figure 1. Although the currents and voltages were not stationary, the measurement was probably satisfactory thanks to the fact that these instruments averaged over time.

Signals were transmitted with the following parameters:

Carrier frequency	225 Hz
M-sequence law	561_8
Number of M-sequences in each transmission	N=1 to 10
Number of digits in the M-sequences	255
Number of carrier frequency cycles per digit	Q = 3 to 16
Commutation time controlling source level	Ts = 1400 to 1600 μs
Modulation angle of the carrier phase	45° to 90°
Sample frequency at the A/D converters	1 to 2 kHz
Depth of submergence	23 to 100 m

Tables 6a and 6b give the parameters of all M-sequence measurements. The source was pre-pressurized at lake-level to about 2.5 atm and 3 atm for measurements at 23 m and 33 m respectively.

It is difficult to obtain accurate estimates of the efficiency of the source and the system (Appendix A).

Figures 17-20 show sections of the hydrophone signals, from M- sequences with the parameters Q = 10, 6, 4 and 3, respectively. Cross-correlation of the reference and the hydrophone signals was done using IAP and K. Metzger's equipment. Correlation data is shown from K. Metzger's equipment.

Figure 21 shows a family of pulses generated with a phase-only matched filter (sharp-processing) with transmitted M-sequences having Q's between 3 and 16. There is a tail for Q's of 3 and 4 (Figures 22 and 23). The tail is probably not due to the reflection from the surface because this reflection arrives about 0.044 s after the main peak. The direct and surface-reflected signals are resolved when the source is submerged to a depth of 100 m (Figure 24). When the source is submerged to a depth of 100 m, the surface reflected signal should arrive about 2×100 m/1440 m s^{-1} = 0.14 s later than the direct arrival.
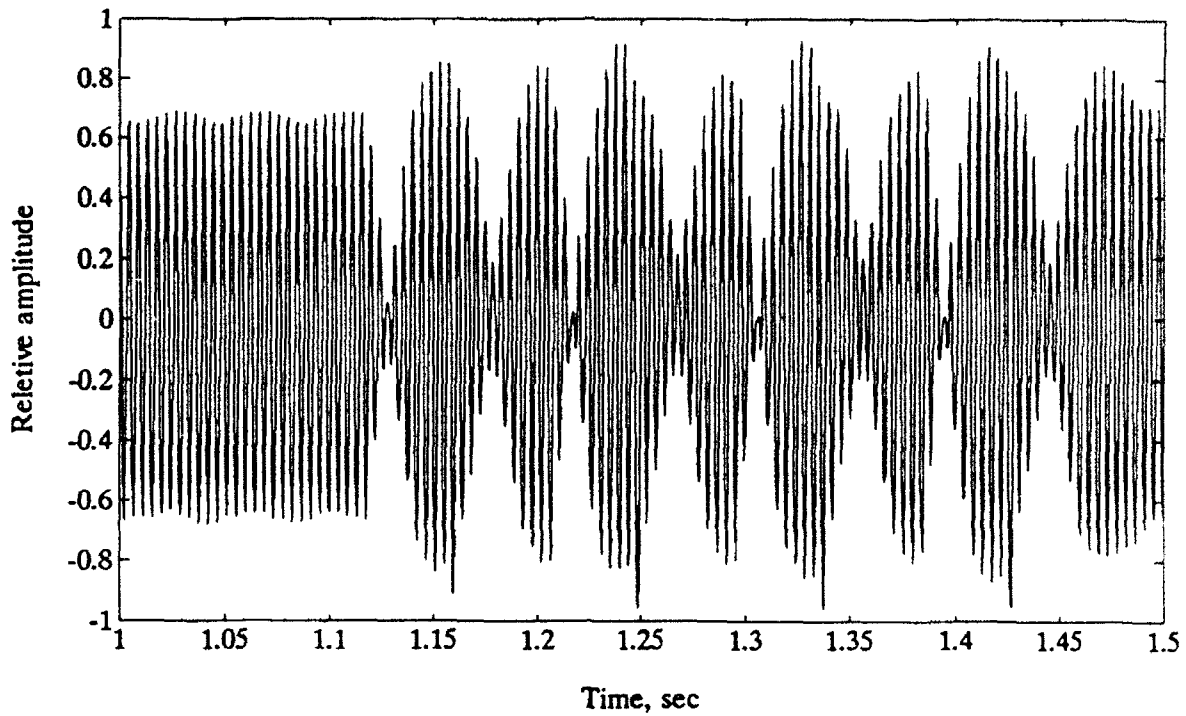
Figure 17: Fragment of the hydrophone received signal
M - sequence, Q = 10.
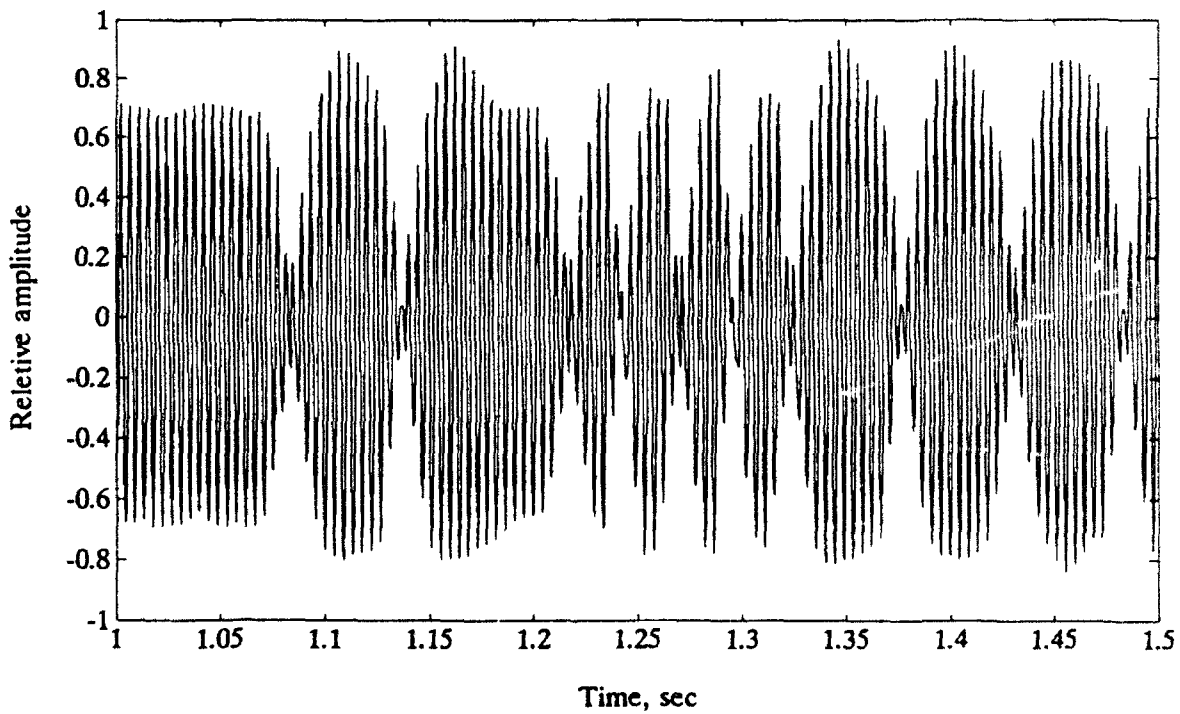
Figure 18: Fragment of the hydrophone received signal
M - sequence, Q = 6.
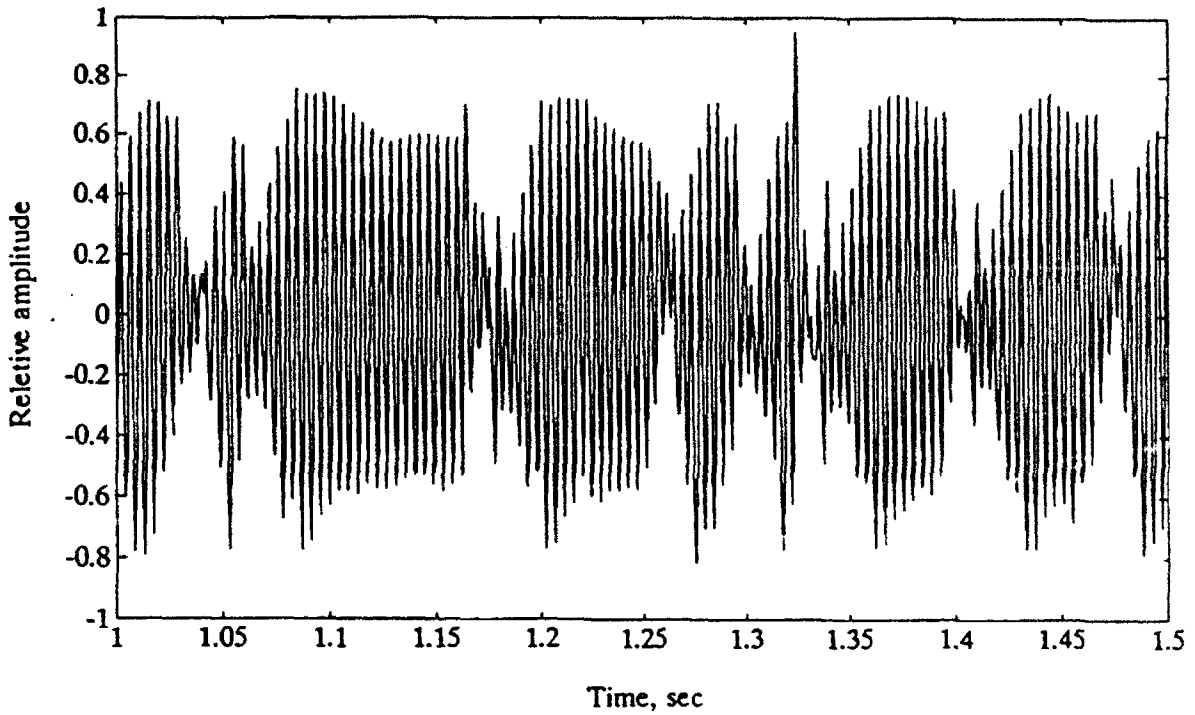
Figure 19: Fragment of the hydrophone received signal
          M - sequence, Q = 4.
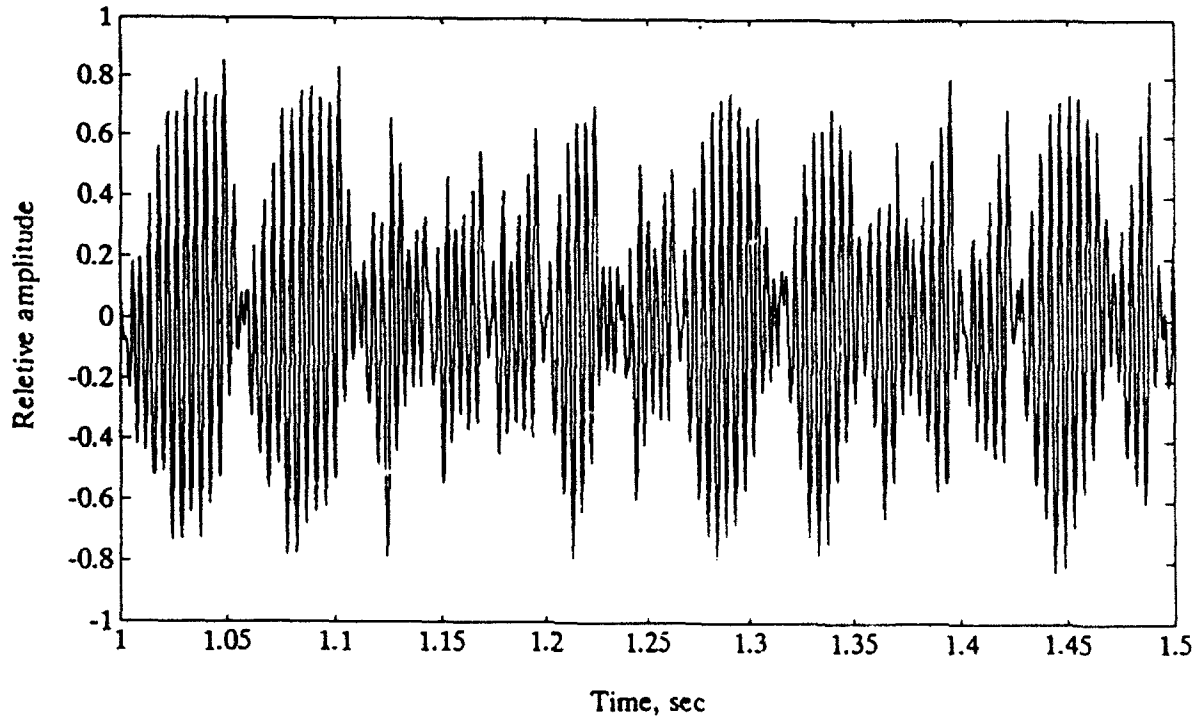
Figure 20: Fragment of the hydrophone received signal
          M - sequence, Q = 3.
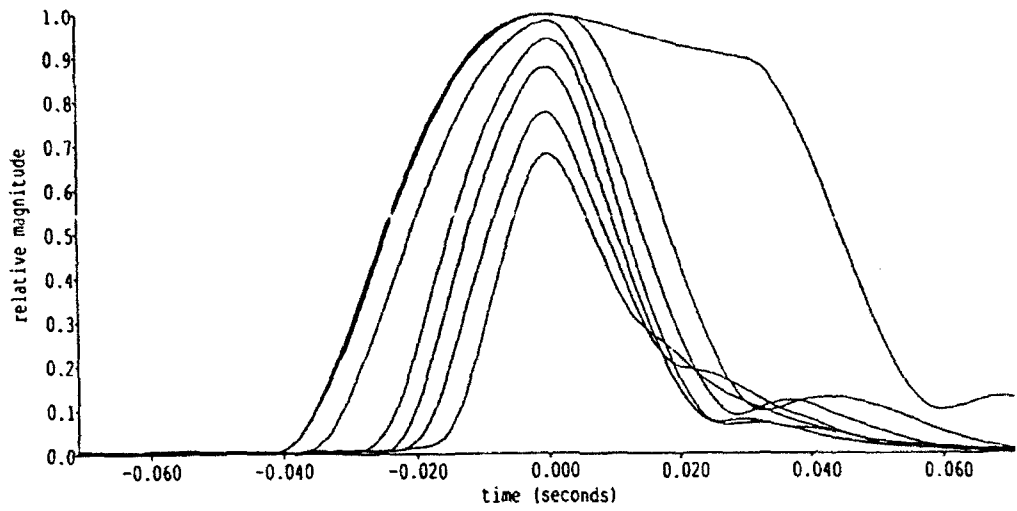
Figure 21: Family of M-sequence convolutions with Q ranging from 3 to 16
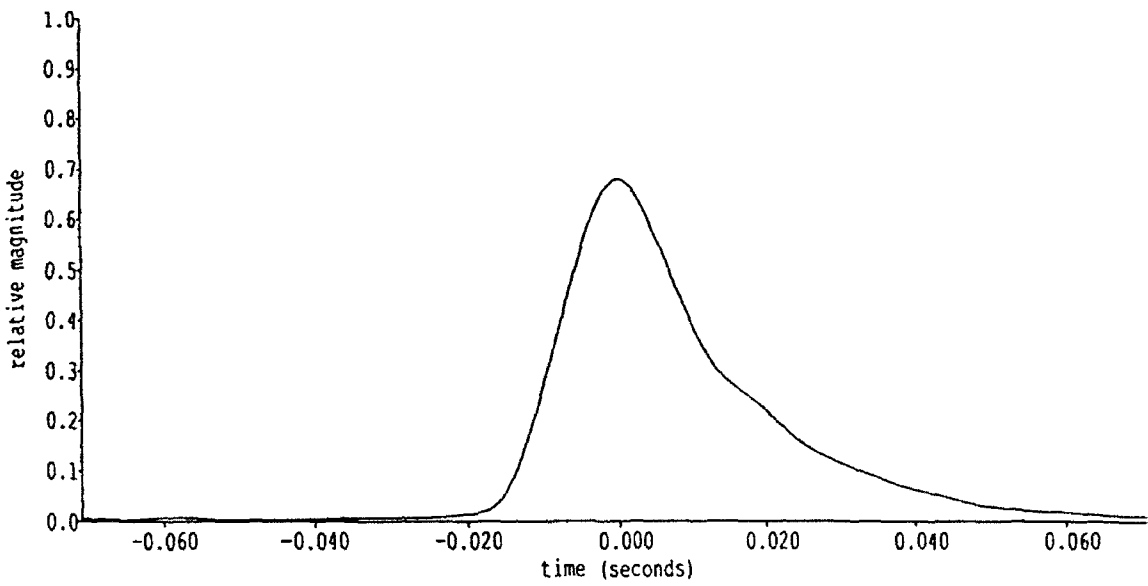
Figure 22: Correlation coefficient for Q = 3.
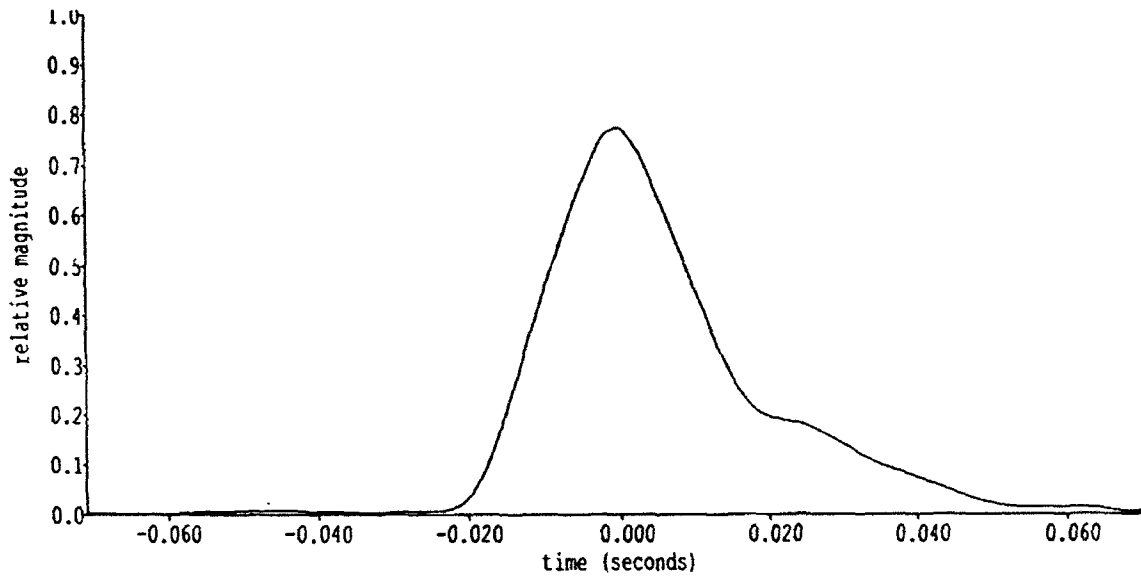
Figure 23: Correlation coefficient for Q = 4
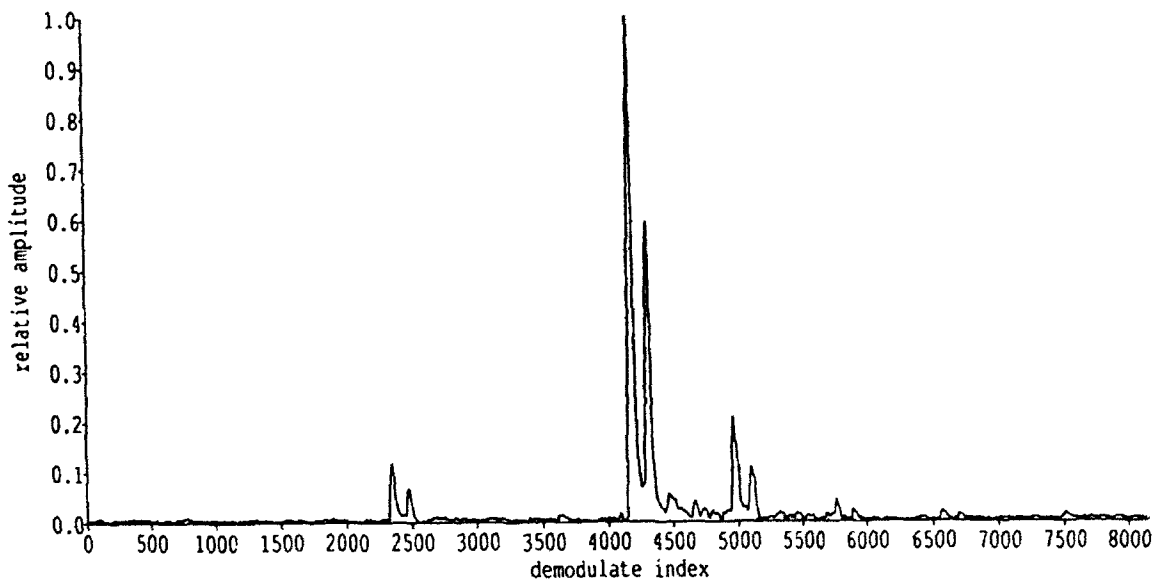
Figure 24: Correlation coefficient for Q=4.
Submergence of the source - 100m.
The sampling frequency of the demodulates is 900 Hz.
The surface arrival is predicted to arrive ~0.14 s
or~126 demodulates after the direct arrival

31

Figures 25 and 26 show the maximum value of the matched-filter output (phase-only filtering) and the width of the correlation peak versus Q respectively. The signal quality is high for values of Q greater than or equal to 4.

The efficiency values shown in Tables 6a and 6b are averaged for each value of Q for tests with and without the pressure compensation system (Figure 27). This figure does not include the efficiency calculation of for hydrophone F37 at a distance of 50 m because of the much larger uncertainty in that particular measurement (Appendix A).

Transmitted signals were subject to linear frequency modulation with and without amplitude tapers according to,

$$A = A0(t)sin(\pi t/T) \ , \tag{6}$$

where T is the signal duration. The algorithm for synthesis of these signals is more complicated than for M-sequences. The algorithm partitions the signal into elementary tones to minimize the number of the emitted tones and it forms each tone using data from the calibration matrix. For signals with a bandwidth of 35 Hz we use the standard calibration matrices described in Section 5. The parameters of the emitted signals are given in Table 7. Figures 28 and 29 show the spectra of signals with linear frequency modulation with and without amplitude modulation.

The tests demonstrate that coded signals can be synthesized with amplitude, phase, and frequency modulations. Using a Q = 4, a temporal resolution of 22 ms is obtained. This resolution is better than the 50 ms resolution required to resolve acoustic multipaths at basin-scales in the northeast Pacific (Spiesberger and Metzger, 1991). The measurements indicate that efficiencies of about 50% are achieved for the system.
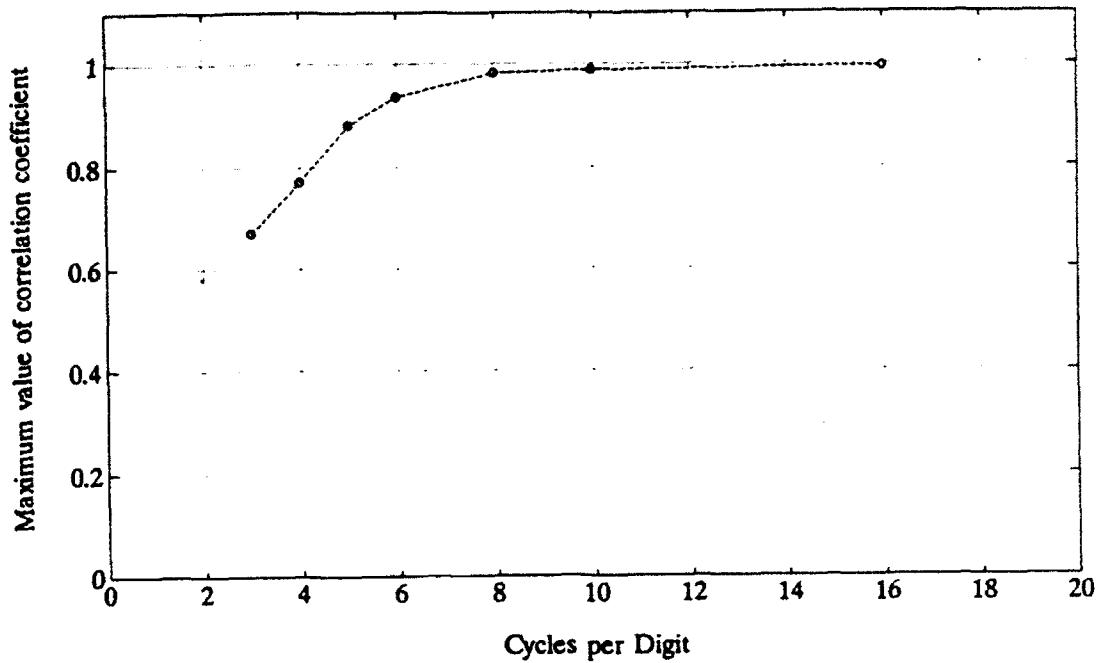
Figure 25: Maximum value of correlation coefficient as a function of Q.
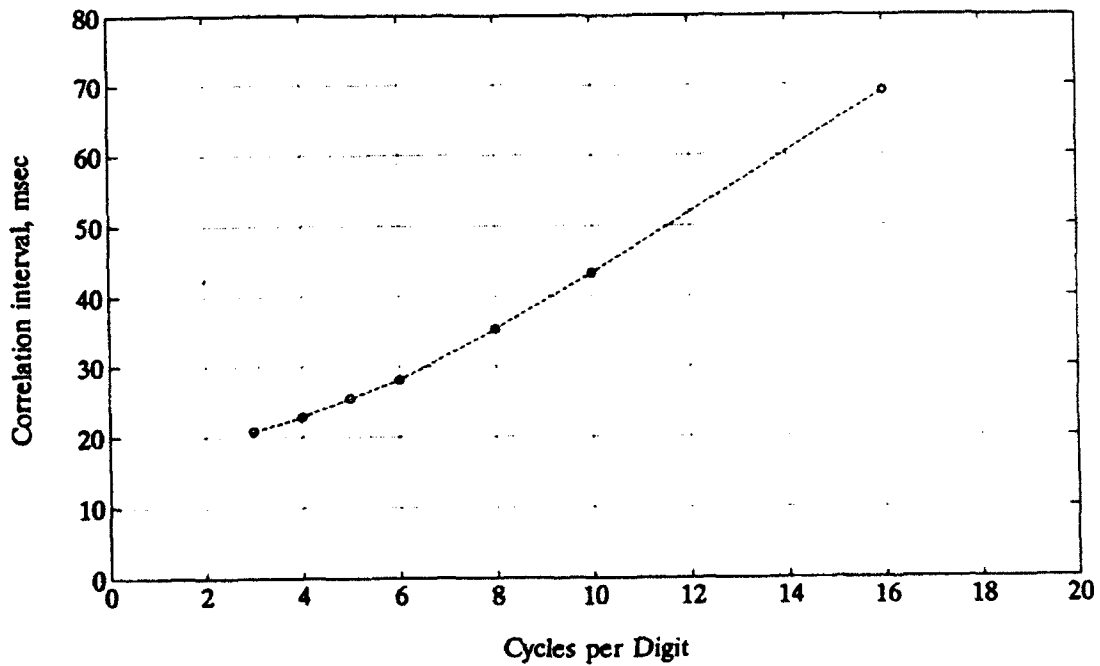
Figure 26: Width of correlation as a function of Q.

33
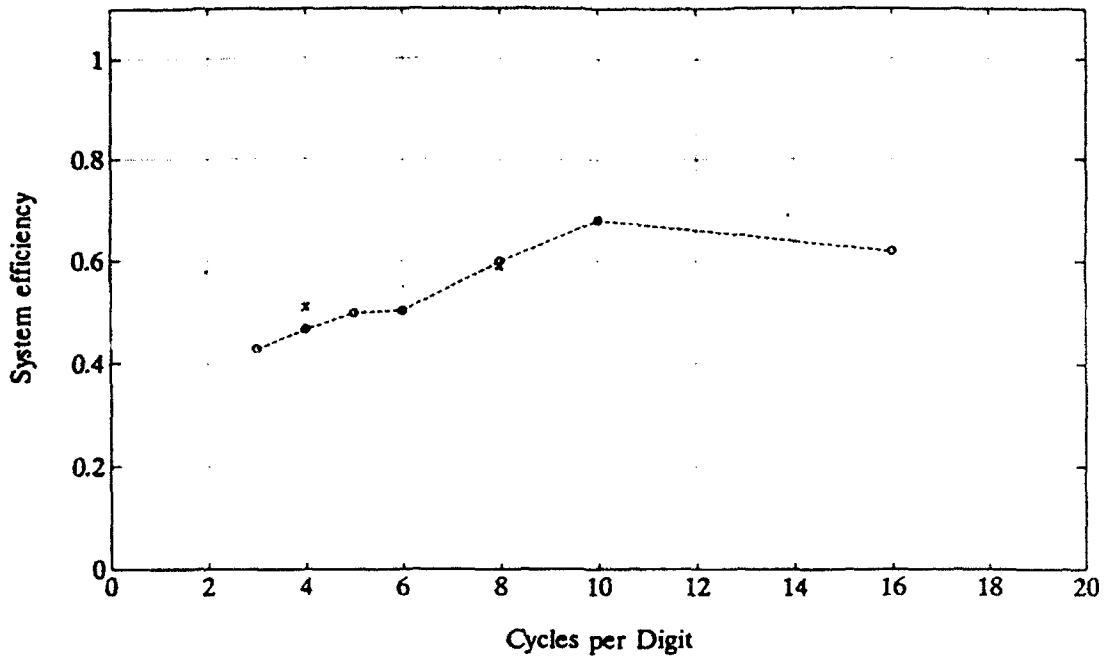
Figure 27: System efficiency as a function of Q.
o: averaged over all tests with equal Q;
x: averaged over all tests with pressure compensation
system and equal Q.
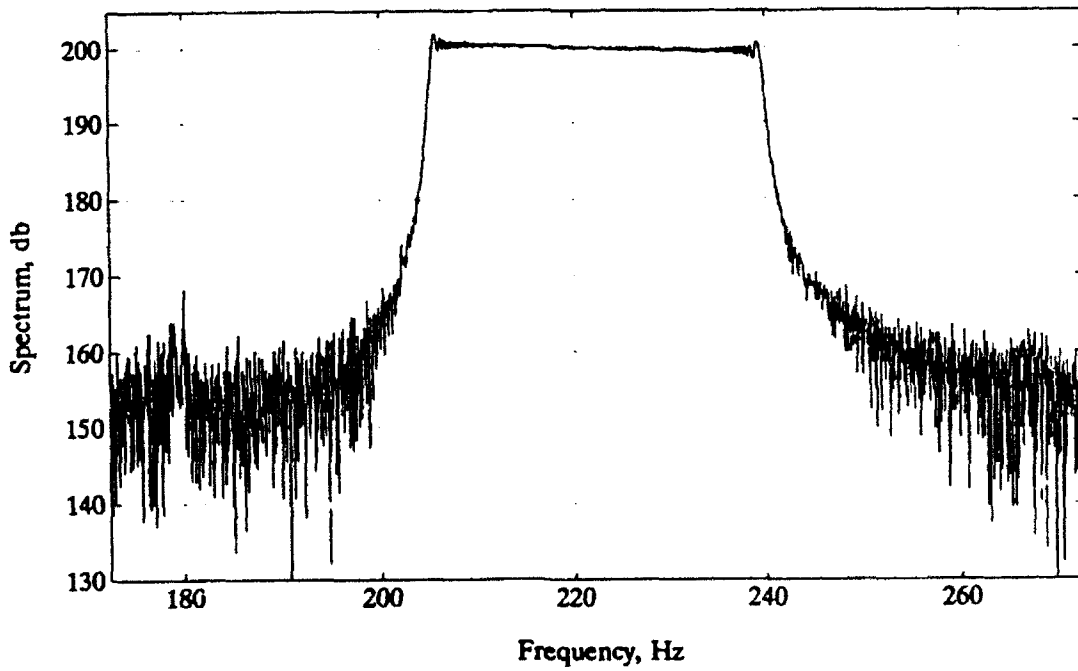
Figure 28: Spectrum of the linear frequency modulated signal
without amplitude modulation.
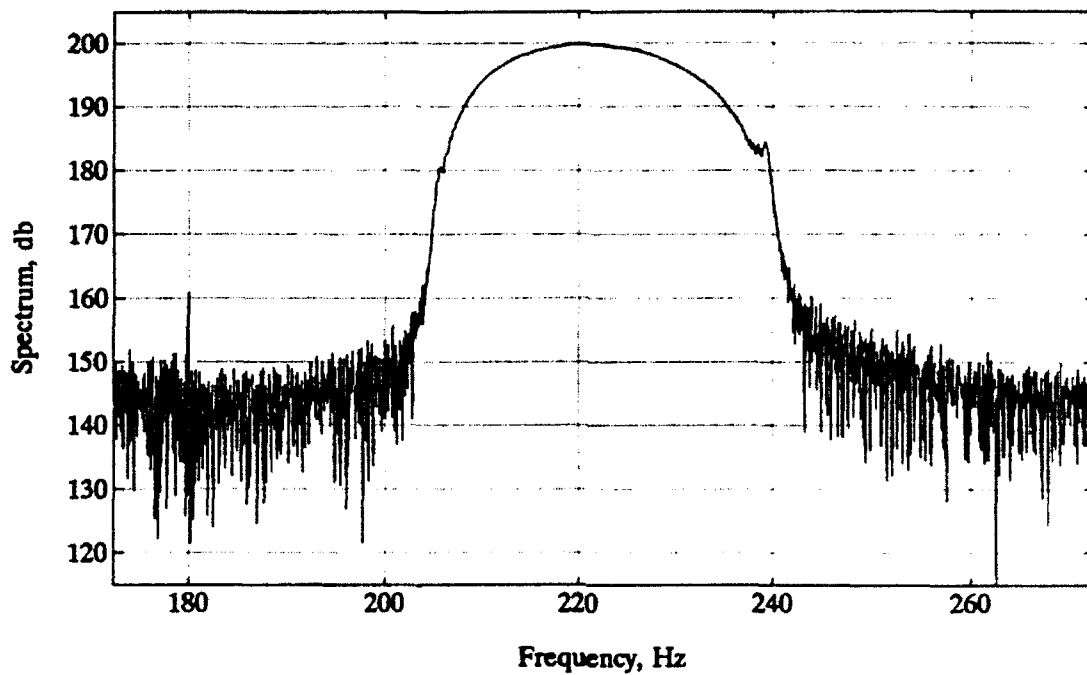
Figure 29: Spectrum of the linear frequency modulated signal with amplitude modulation.

Table 6a. M-sequence measurements. The columns give the source depth, the number of digits in the M-sequence (n), the number of M-sequence periods transmitted (N), the number of cycles of carrier per digit of the M-sequence (Q), the phase angle used to modulate the M-sequence, the source level of the transmission relative to 1 μPa @ 1 m, and the fractional efficiency of the source and the driving equipment (E_c). The M-sequence law is 561_8 according to K. Metzger's notation and law (8,4,3,2) according to the IAP notation. The carrier frequency for all transmissions is 225 Hz. The geometry of the test is shown in Figure 6b except the distance between the source and the hydrophones is 1.99 m. Calculations for SL are taken from the average source levels derived from the F37 hydrophones. E_c is calculated from hydrophones F37, serial # A62 and serial #280 respectively with voltages on hydrophone outputs measured with the 8506A true rms meter. The average value of E_c is shown. Errors for the efficiency might be about 25 % (Appendix A).

| #	Depth (m)	n	N	Q	Angle (deg)	SL (dB)	E_c F37 A62	E_c F37 280	avg	Notes
1	23	255	1	10	86.42					
2	23	31	1	10						
3	23	31	1	10	90.00					
4	23	31	1	10	45.00					
5	23	31	1	10	45.00					
6	23	255	5	10	86.417					
7	23	255	2	10	86.417					
8	23	255	1	10	90.00					
9	23	31	5	10	90.00					
10	23	255	5	8	86.417					
11	23	255	5	6	86.417					
12	23	255	5	4	86.417					
13	23	255	5	3	86.417					
14	23	255	5	4	90.000					
15	23	255	5	4	86.417	197.40	0.40	0.54	0.45	
16	23	255	5	8	86.417	198.00	0.45	0.58	0.52	
17	23	255	5	8	86.417	197.50	0.57	0.73	0.65	
18	23	255	5	5	86.417	197.60	0.42	0.54	0.48	
19	23	255	5	6	86.417	197.60	0.41	0.55	0.48	
20	23	255	5	7	86.417	197.70	0.42	0.56	0.49	
21	23	255	5	16	86.417	198.20	0.48	0.63	0.56	
22	23	255	5	4	86.417	196.80	0.34	0.45	0.40	
23	23	255	5	3	86.417	197.00	0.35	0.48	0.42	

Table 6b. Same as Table 6a. For tests 32 through 41, the geometry is shown in Figure 6b and the SL are computed in part using hydrophone F37, serial #280. PCS indicates a pressure compensation system is used. KMG indicates K. Metzger's BCSG80 M-sequence generator is used.

#	Depth (m)	n	N	Q	Angle (deg)	SL (dB)	E_c F37 A62	E_c F37 280	avg	Notes
24	33	255	2	16	86.417	198.50	0.60	0.77	0.69	
25	33	255	2	10	86.417	198.40	0.59	0.77	0.68	
26	33	255	2	8	86.417	198.20	0.55	0.75	0.65	
27	33	255	5	6	86.417	198.00	0.44	0.61	0.53	
28	33	255	5	5	86.417	197.80	0.42	0.57	0.50	
29	33	255	5	4	86.417	197.50	0.39	0.53	0.46	
30	33	255	5	3	86.417	197.20	0.38	0.50	0.44	
31	33	255	5	4	84.375	197.60	0.41	0.57	0.49	KMG
32	45	255	5	4	86.417	197.90		0.47		PCS
33	45	255	5	8	86.417	198.50		0.55		PCS
34	45	255	5	8	84.375	198.60		0.56		KMG,PCS
35	45	255	5	4	84.375	198.00		0.50		KMG,PCS
36	75	255	5	4	86.417	198.10		0.50		PCS
37	75	255	5	4	84.375	198.10		0.50		KMG,PCS
38	100	255	5	4	86.417	198.40		0.54		PCS
39	100	255	5	8	86.417	199.00		0.63		PCS
40	100	255	5	4	84.375	198.20		0.53		KMG,PCS
41	100	255	5	8	84.375	199.00		0.62		KMG,PCS

Table 7. Parameters used for signals generated with a linear frequency modulation. See Equation (6) for a description of the variables describing the frequency sweep.

f_0 (Hz)	f_1 (Hz)	T (s)	Amplitude modulation	SL (dB)
205	240	100	no	200
205	240	50	no	200
205	240	50	yes	200

7. PRESSURE COMPENSATION SYSTEM AND COLD START TEST

Operation of the source with a compensator was investigated at a depth of up to 100 m. The inductance of the source field coil was measured as a function of depth (Fig. 30). The inductance indicates the extent to which internal and external pressures are equalized at the source since the coil inductance is inversely proportional to the core gap and the gap depends on the flexibility of the source membranes. The inductance of the compensated source, measured in the air together with a cable of length 200 m, was 45.1 mH. After this, the source was connected to the compensator and pumped with gas (dry air could be used) to 4 atm. The inductance decreased to 27.5 mH. The inductance must increase to an equilibrium value of 45.1 mH when the source is placed at a depth of 40 m. After the source is brought to the depth where its internal pressure equals the external pressure, the inductance can undergo slight oscillations.

The depth was quickly changed at 10 m steps. The time of inductance relaxation was about 3 minutes (not shown). Figure 30 shows the dependence of the inductance as a function of depth. When the source was submerged to a depth greater than 40 m, slight inductance oscillations (± 0.5 mH) were detected over a period of about 3 minutes due to pressure dis-equilibrium (not shown). Therefore, a sudden pressure differential of 1 atm relaxes to equilibrium in 3 minutes.

In order to estimate the accuracy to which the compensator sustained the pressure difference the following experiment was performed. The inductance of the un-pumped source on the deck (L = 39 mH) was measured. Then the source without the PCS was pumped with air to pressure, P0, corresponding to the hydrostatic pressure at the depth of submergence. Thereafter we measured the coil inductance at different depths as the source was submerged. The results of these measurements are given in Figure 31. Pressure imbalances as great as 0.1 atm lead to a change of inductance by 1 mH.

The coil inductance is within ± 0.5 mH of equilibrium when the pressure compensator is used (Figure 30). Therefore, the accuracy in maintaining the pressure difference by use of the compensator is ± 0.05 atm.

The transmission characteristics were investigated when the pressure inside the source was not equal to the outside pressure. The source was calibrated without the compensator at several depths from 29.4 m to 36.6 m, which corresponds to a pressure differential of ± 0.3 atm. The use of an un-compensated source, which changes the core gap, means that the a higher or lower coil current is required to force oscillation of the source membranes. In other words, dis-equilibrium leads to changes in the dependence of source level with coil current. The input parameter is Ts rather than the current. The source (radiation) level does not change much under the stabilizing action of the inverter which controls Ts. Consequently, the dependence of the source level on frequency changes little at $Ts = $ constant (Figures 32, 33, and 34). An inaccuracy in compensation of about 0.3 atm is unessential to the source operation. The pressure difference at which these sources

38
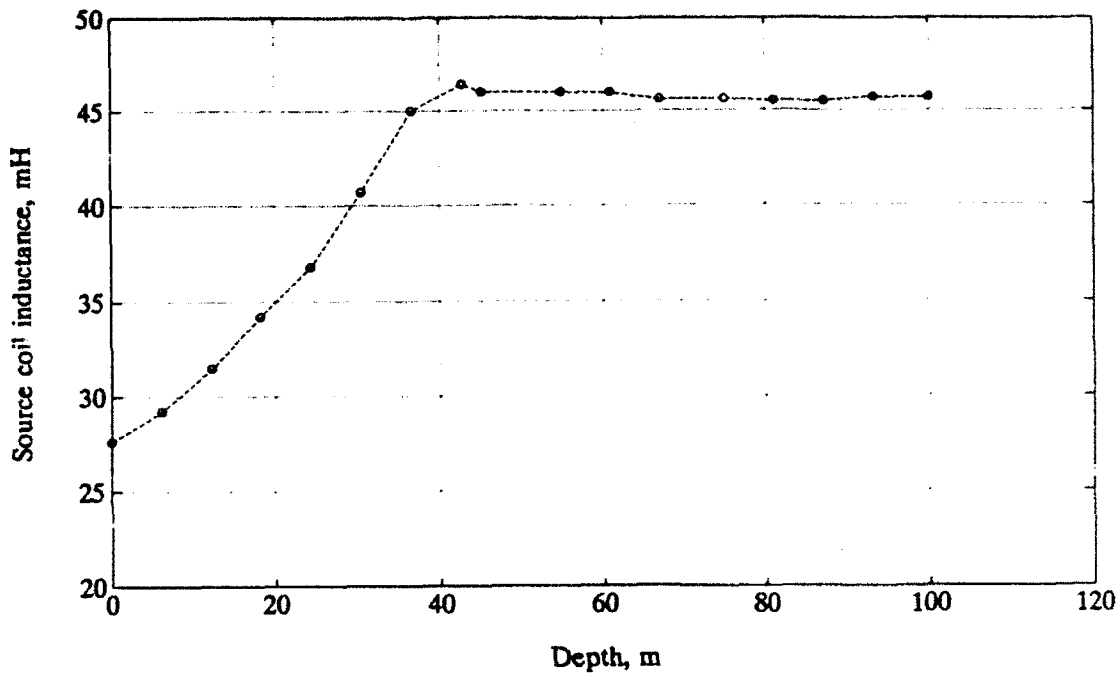
Figure 30: Source coil inductance as a function of depth.
Source with pressure compensation system.
Po = 4 atm, initial pressure inside the
compensation system.
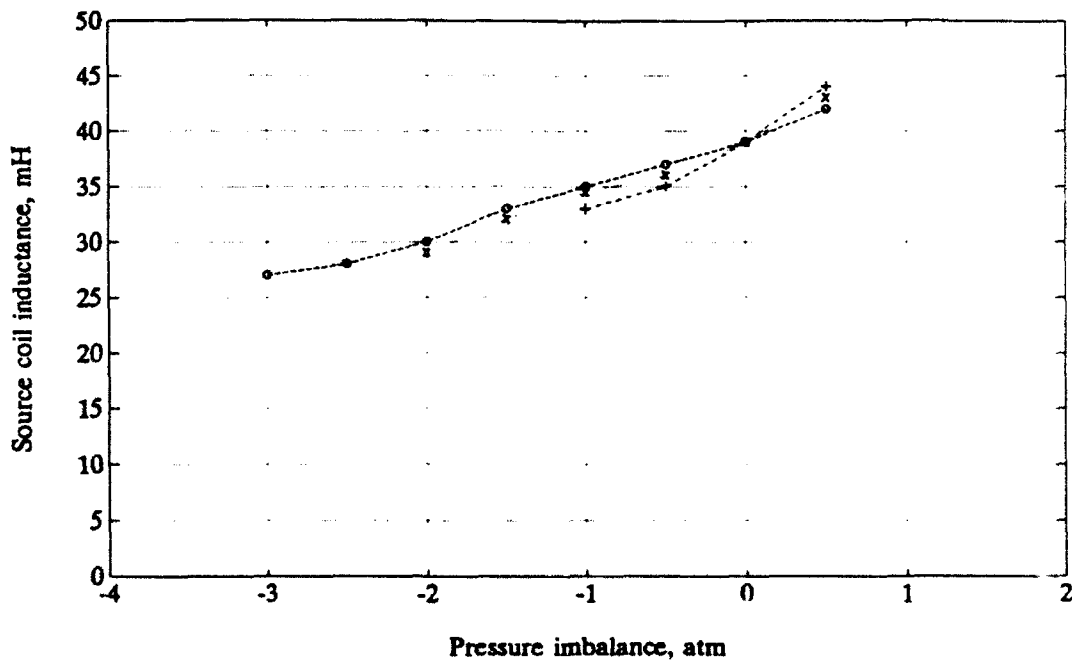
Figure 31: Source coil inductance as a function of pressure
imbalance (the difference between external and
internal pressure). Source without the compensator.
P0 - initial pressure inside the source;
o is Po = 3 atm; x is Po = 2.3 atm; + is Po = 1 atm
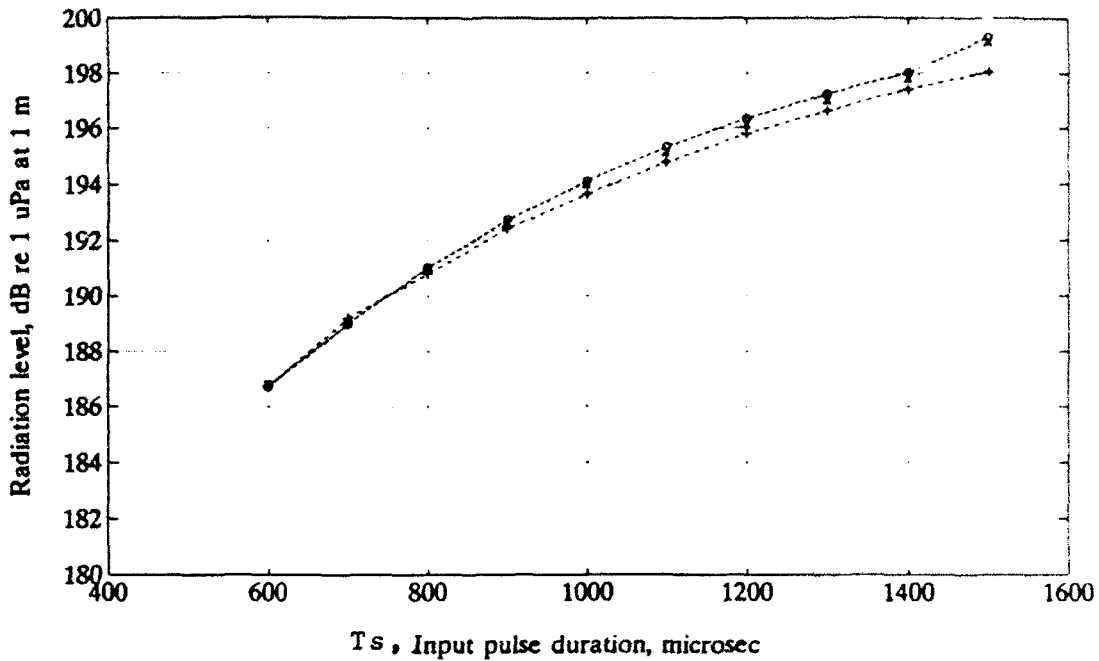
Figure 32: Radiation level as a function of input pulse duration.
Source without a compensator. F = 225 Hz,
Frequency; depth : + is 36.6 m, x = 33 m, o = 29.4 m
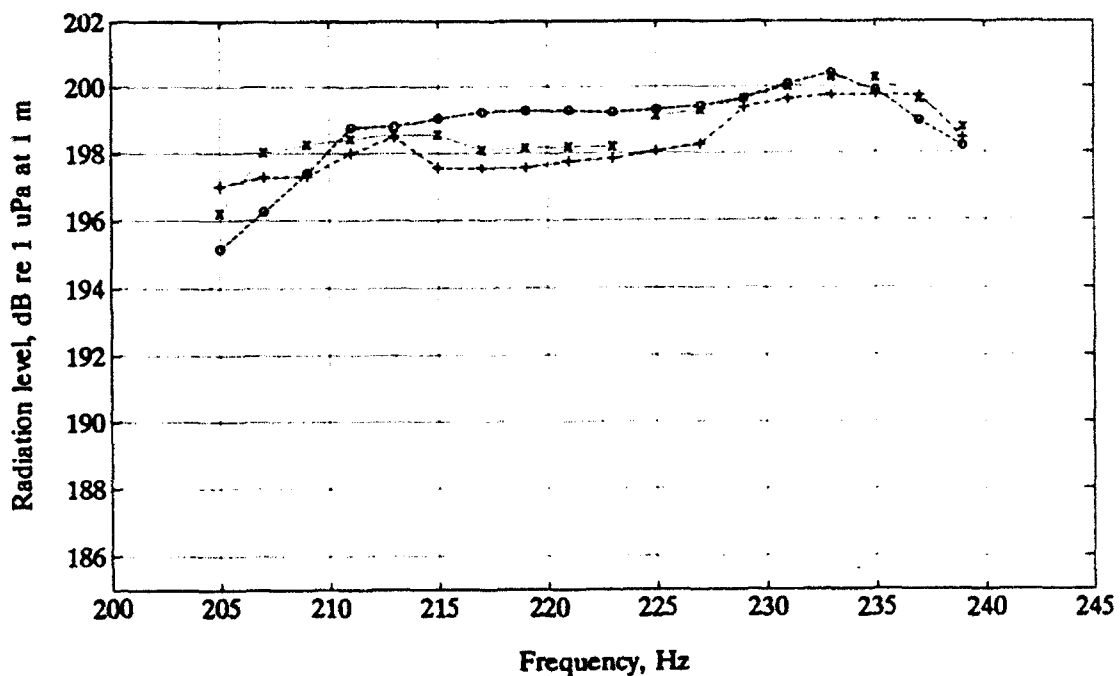
Figure 33: Radiation level as a function of frequency.
Source without a compensator. Ts = 1500 microsec,
input pulse duration depth: + is 36.6 m, x is 33 m,
o is 29.4 m.
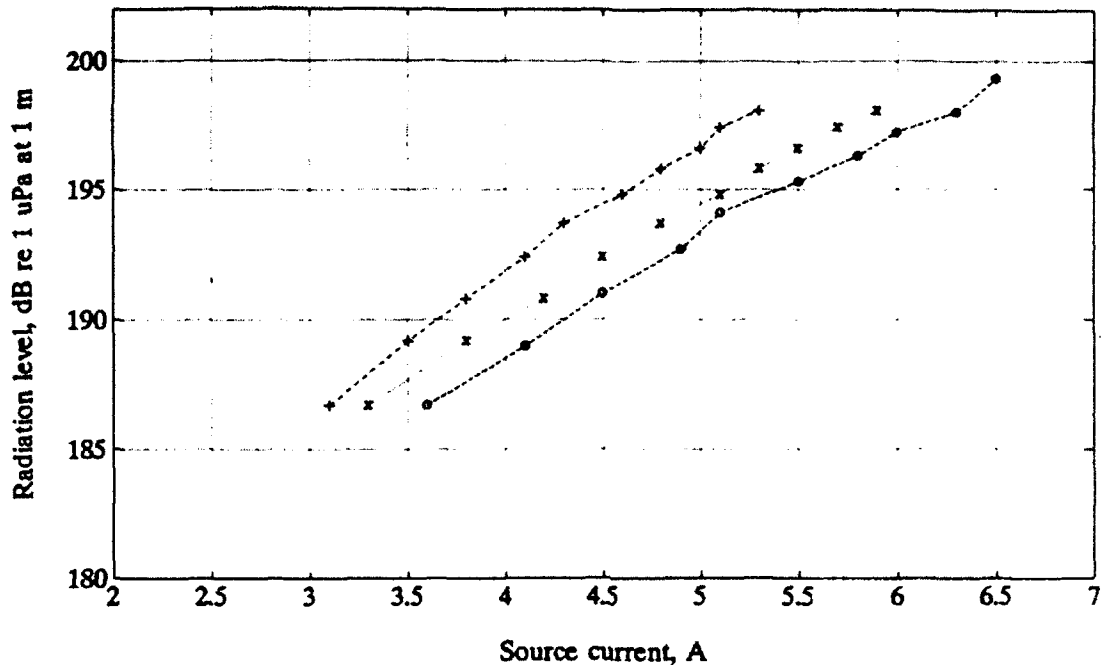
Figure 34: Radiation level as a function of source col current.
Source without a compensator. F = 225 Hz, frequency;
Depth: + is 36.6 m, x is 33 m, o is 29.4 m.
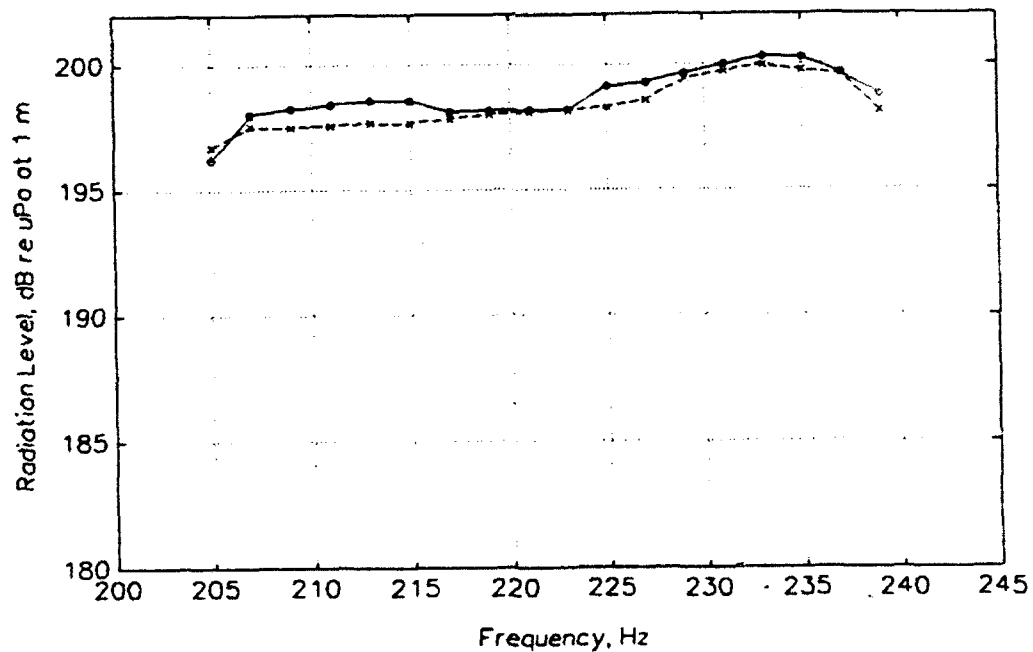
Figure 35: Frequency dependence of radiation level at
constant Ts with and without PCS.
0 - without PCS, H = 33 m; x - with PCS, H = 45 m.

are serviceable is ± 1 atm, and the compensator sustains the pressure difference ± 0.05 atm.

The ability of the system to transmit properly after a long break ("cold start") was tested. At the start of each working day on the NUSC barge, a calibration matrix was measured on the source which was left in the water overnight. Measurements show that a break of about 15 hrs does not influence the source radiation characteristics (not shown).

8. CONCLUSIONS

The main results are:

(a) The Russian and American specialists developed methods for testing low-frequency hydroacoustic sources and emitting systems. In the course of further collaboration in the field of the ocean acoustic tomography, these methods can be used as a basis for independent estimation of different sources.

(b) The method and equipment for automated measurement of the calibration matrices for determination of the main acoustic and electric characteristics of the transmission system have been tested experimentally. In the range 205 - 240 Hz, the frequency response of the transmission system equipped with a compensation system is flat ($\pm$ 1.5 dB on the average). At resonance, the efficiency of the transmission system with the PCS and the efficiency of the source in this system is about 66% and 75% respectively at a source level of about 200 dB.

(c) A method of determining the characteristics of the hydrostatic pressure compensation system and the influence of the compensator on the transmissions was tested. The characteristics of the calibration matrices changed little when the compensator was attached to the source. The rate of compensation of the internal and external hydrostatic pressure is approximately $V'c$ = 0.005 atm/s, and the pressure compensation accuracy, dP = 0.05 atm, is high enough to ensure serviceability for uses on moorings.

(d) The transmission system is insensitive to the starting condition, e.g. a "cold start" condition.

(e) Confirmation of the source's reliability ($\sim 3 \times 10^8$ cycles) requires long-term tests not performed in the summer of 1992. The total time that one of the sources was used in the summer of 1992 was about 10 hours which is about 8.1×10^6 cycles of carrier at 225 Hz.

(f) We verified that the IAP resonant low frequency sources, with dynamic electric control, emit coded signals suitable for tomographically monitoring climatic temperature changes over ocean basins. With a PCS at 198 dB, and a pulse resolution of 35.3 ms (Q=8) and 22.8 ms (Q=4), the system has an average efficiency of about 59% and 50% respectively. The efficiency measurements are difficult to make, so these efficiency estimates should not be taken as definitive. Whatever the efficiency really is, it can be increased by 6% by using a power cable shorter than we used at Lake Seneca (200 m).

(g) The transmission system synthesizes a wide class of coded signals using amplitude, phase, and frequency modulations.

REFERENCES

Bogolubov, B.N., Okomelkov, A.V., Ostrovsky, L.A., and Slavinsky, M.M., (1986). Interaction of the resonance acoustic monopoles, Akustichesky Zhurnal, v32, 1, 15-20.

Slavinsky, M.M., Bogolubov, B., and Spiesberger, J.L., (1992). Low-frequency high efficiency sources for acoustic monitoring of climatic temperature changes in ocean basins, Acoustical Society of America conference 31 October - 4 November, New Orleans, J. Acoust. Soc. Am., **92**, No. 4, Pt. 2, p. 2349, October (1992).

Spiesberger, J. L., (1992). Listening for climatic temperature change in the ocean, *Proceedings, Oceanology 92 conference*, Brighton, England, March.

Spiesberger, J. L., (1993). Is it cheaper to map Rossby waves in the global ocean than in the global atmosphere?, in press, *Journal of Marine Environmental Engineering*, 1.

Spiesberger, J. L., and Bowlin, J. B., (1993). A telemetry theory for ocean acoustic tomography: Real time monitoring, in press, *Journal of Marine Environmental Engineering*, 1.

Spiesberger, J. L., and Metzger, K., (1992). Basin scale ocean monitoring with acoustic thermometers, *Oceanography*, **5**, 92-98.

Urick, R. J., (1983). Principles of underwater sound, 3rd edition, McGraw-Hill, pp. 423.

APPENDIX A: EFFICIENCY ESTIMATES

It is difficult to obtain accurate estimates of the efficiency with which electrical energy is converted to acoustic energy. The following describe the challenges in obtaining this estimate.

1. The U.S. Navy hydrophones (type F37) are calibrated to within about 1 dB. Let the measured sound pressure level be D with error δD in dB. The measurement of acoustic intensity equals,

$$I = I_{ref} 10^{0.1D} 10^{0.1\delta D} \text{ W cm}^{-2} , \tag{A1}$$

where $I_{ref} = 1 \ \mu\text{Pa} = 0.67 \times 10^{-22} \text{ W cm}^{-2}$ (Urick, 1983). The fractional change in the intensity due to measurement error of the source level is,

$$\frac{\delta I}{I} = (10^{0.1D} - 1) . \tag{A2}$$

For $\delta D = 1$ dB, the fractional change in the intensity due to measurement error of the source level is 0.26. In other words, a 1 dB error in calibration leads to an output power change of 26%.

2. Assuming spherical spreading of acoustic energy, the intensity at distance r (m) from the center of the source is related to the intensity at a distance of 1 m by,

$$I(r = 1) = r^2 I(r) . \tag{A3}$$

The fractional change in inferred intensity at 1 m due to error, δr in the measurement of the range is,

$$\frac{\delta I(1)}{I(1)} \approx \frac{2\delta r}{r} . \tag{A4}$$

Figure 6 has $r \cong 2$ m. If $\delta r = 0.05$ m, the fractional change in inferred intensity at 1 m is 0.05.

3. Reflections from the surface, bottom, and underwater objects lead to aberrations in the estimates of efficiency. We calculate the worse case interference between the direct and reflected paths between the source and a hydrophone. Let the direct and reflected paths have distances r_d and r_r respectively. Assuming specular reflection and assuming a reflection coefficient of unity, the pressure at the hydrophone is proportional to the real part of,

$$p = \frac{1}{r_d} \exp(ikr_d) + \frac{1}{r_r} \exp(ikr_r) ,$$

where the dependence on time is not indicated but is sinusoidal and where the acoustic wavenumber is k. The intensity is,

$$p^2 = \frac{1}{r_d^2} + \frac{1}{r_r^2} + \frac{2}{r_d r_r} \cos k(r_d - r_r) ,$$

which has maximum interference when $k(r_d - r_r) = 0$ or an integer multiple of π. The percent error due to the interference is therefore,

$$E = 100\frac{\frac{1}{r_r^2} + \frac{2}{r_d r_r}}{\frac{1}{r_d^2}} = 100\left(\frac{2r_d}{r_r} + \frac{r_d^2}{r_r^2}\right) \quad . \tag{A5}$$

For $r_d = 2$ m and $r_r = 46$ m (23 m from the surface), $E \cong 9\%$. The aberration may be worse if nearby objects are resonated by the acoustic transmissions. We do not have any estimates for the magnitude of this effect. There was a large sphere in the vicinity of the source. The diameter of the sphere is about 7 m and its point of closest approach is about 18 m with the source at a depth of 30 m.

The overall accuracy of our efficiency estimates is unknown. At best, the efficiency estimates cannot be better than possible with a ± 1 dB uncertainty in the hydrophone calibrations which implies an error in the output power of about $\pm 26\%$.

Efficiency measurement at 50 m distance

A measurement of the source was made with the F37 serial #A62 hydrophone at a distance of about 50 m for test 40 in table 6b. This data is not shown in that table

The F37 serial #A62 hydrophone was suspended at a depth of 50 m and the source was suspended at a depth of 100 m. The horizontal separation between the cables was 14.53 m at the surface. Assuming the cables hung vertically, the distance between the source and the hydrophone is 52.07 m. The other hydrophone was at a distance of 2.03 m from the source. The distance between the source and the far hydrophone was independently measured to be 52.48 m from the arrival time difference of the acoustic pulse at the near and far hydrophone. Using Equation (A5), the percent error in the efficiency measurement from this hydrophone is $E \cong 76\%$.

After passing the signal from the far phone through the Ithaco amplifier at 45 dB gain, the signal on the far hydrophone was 2.09 dBV, giving an inferred source level of,

$$2.09 + 204.3 + 20log_{10}\frac{52.07 \text{ m}}{1 \text{ m}} - 45 = 195.72 \text{ dB} \quad .$$

This is 333 watts acoustic or an efficiency of 30% since the input was 1121 watts. If the distance is 52.48 m instead of 52.07 m, the source level is 195.79 dB at 1 m or 338 watts or still about 30% $\pm$ 76%.

In this test, an Ithaco amplifier was used to boost the output of the F37 serial#62 by about 45 dB. We did not check the accuracy of this amplifier, but if the amplifier was in error by 0.5 dB, the output power is in error by 12%.

DOCUMENT LIBRARY

February 5, 1993

Distribution List for Technical Report Exchange

University of California, San Diego
SIO Library 0175C (TRC)
9500 Gilman Drive
La Jolla, CA 92093-0175

Hancock Library of Biology &
  Oceanography
Alan Hancock Laboratory
University of Southern California
University Park
Los Angeles, CA 90089-0371

Gifts & Exchanges
Library
Bedford Institute of Oceanography
P.O. Box 1006
Dartmouth, NS, B2Y 4A2, CANADA

Office of the International
  Ice Patrol
c/o Coast Guard R & D Center
Avery Point
Groton, CT 06340

NOAA/EDIS Miami Library Center
4301 Rickenbacker Causeway
Miami, FL 33149

Library
Skidaway Institute of Oceanography
P.O. Box 13687
Savannah, GA 31416

Institute of Geophysics
University of Hawaii
Library Room 252
2525 Correa Road
Honolulu, HI 96822

Marine Resources Information Center
Building E38-320
MIT
Cambridge, MA 02139

Library
Lamont-Doherty Geological
  Observatory
Columbia University
Palisades, NY 10964

Library
Serials Department
Oregon State University
Corvallis, OR 97331

Pell Marine Science Library
University of Rhode Island
Narragansett Bay Campus
Narragansett, RI 02882

Working Collection
Texas A&M University
Dept. of Oceanography
College Station, TX 77843

Fisheries-Oceanography Library
151 Oceanography Teaching Bldg.
University of Washington
Seattle, WA 98195

Library
R.S.M.A.S.
University of Miami
4600 Rickenbacker Causeway
Miami, FL 33149

Maury Oceanographic Library
Naval Oceanographic Office
Stennis Space Center
NSTL, MS 39522-5001

Marine Sciences Collection
Mayaguez Campus Library
University of Puerto Rico
Mayaguez, Puerto Rico 00708

Library
Institute of Oceanographic Sciences
Deacon Laboratory
Wormley, Godalming
Surrey GU8 5UB
UNITED KINGDOM

The Librarian
CSIRO Marine Laboratories
G.P.O. Box 1538
Hobart, Tasmania
AUSTRALIA 7001

Library
Proudman Oceanographic Laboratory
Bidston Observatory
Birkenhead
Merseyside L43 7 RA
UNITED KINGDOM

IFREMER
Centre de Brest
Service Documentation - Publications
BP 70 29280 PLOUZANE
FRANCE

50272-101

REPORT DOCUMENTATION PAGE	1. REPORT NO. WHOI-93-09	2.	3. Recipient's Accession No.
4. Title and Subtitle Evaluation of Electromagnetic Source for Ocean Climate Acoustic Thermometry at Lake Seneca			**5. Report Date** February 1993
			6.
7. Author(s) Mark Slavinsky, Boris Bogolubov, Igor Alelekov, Konstantin Pigalov, John L. Spiesberger and Paul Boutin			**8. Performing Organization Rept. No.** WHOI-93-09
9. Performing Organization Name and Address Woods Hole Oceanographic Institution Woods Hole, Massachusetts 02543			**10. Project/Task/Work Unit No.**
			11. Contract(C) or Grant(G) No. (C) N00014-92-J-1222 (G)
12. Sponsoring Organization Name and Address Office of Naval Research			**13. Type of Report & Period Covered** Technical Report
			14.

16. Abstract (Limit: 200 words)

A compact electromagnetic monopole source, requiring pressure equalization, was evaluated at the Naval Underwater Systems Center at Lake Seneca during July 1992 by scientists from the Institute of Applied Physics of the Russian Academy of Sciences (IAP RAS) and from the Woods Hole Oceanographic Institution and other American organizations. The titanium source was developed at the IAP RAS. The source has a mass of 123 kg and a diameter of .54 m. The source cannot be thought of as a single unit; rather the characteristics of the transmitted signal depend on a transmission system consisting of the source, the power amplifier, and a computer. The computer and the amplifier send specially adapted signals to the source to produce the desired acoustic signals. Measurements indicate the acoustic system as a center frequence of 225 Hz, a bandwidth of about 50 Hz, an associated pulse resolution of about 0.02 s, a source level of about 198 dB re 1 μPa @ 1 m, with an efficiency of about 50%. The system has an efficiency of about 67% near 225 Hz, the resonant frequence. The source is suitable for mounting on autonomous ocean moorings for several years as part of a system of monitoring climatic temperature changes over basin scales.

17. Document Analysis   a. Descriptors

acoustic tomography
ocean acoustic thermometers
acoustic monopull source

b. Identifiers/Open-Ended Terms

c. COSATI Field/Group

18. Availability Statement Approved for public release; distribution unlimited.	19. Security Class (This Report) UNCLASSIFIED	21. No. of Pages 48
	20. Security Class (This Page)	22. Price

(See ANSI-Z39.18)   *See Instructions on Reverse*   OPTIONAL FORM 272 (4-77)
(Formerly NTIS-35)
Department of Commerce